EXPERIMENTAL INVESTIGATION OF THE EFFECTS OF TIP INJECTION ON THE CHARACTERISTICS OF THE TIP VORTEX ON A MODEL WIND TURBINE

A THESIS SUBMITTED TO
THE GRADUATE SCHOOL OF NATURAL AND APPLIED SCIENCES
OF
MIDDLE EAST TECHNICAL UNIVERSITY

BY

EZGİ ANIK

IN PARTIAL FULFILLMENT OF THE REQUIREMENTS
FOR
THE DEGREE OF MASTER OF SCIENCE
IN
AEROSAPCE ENGINEERING

FEBRUARY 2015

Approval of the thesis:

EXPERIMENTAL INVESTIGATION OF THE EFFECTS OF TIP INJECTION ON THE CHARACTERISTICS OF THE TIP VORTEX ON A MODEL WIND TURBINE

Submitted by **EZGİ ANIK** in partial fulfillment of the requirements for the degree of **Master of Science in Aerospace Engineering Department, Middle East Technical University** by,

Prof. Dr. Gülbin Dural Ünver
Dean, Graduate School of **Natural and Applied Sciences** _____

Prof. Dr. Ozan Tekinalp
Head of Department, **Aerospace Engineering** _____

Assoc. Prof. Dr. Oğuz Uzol
Supervisor, **Aerospace Engineering Dept., METU** _____

Examining Committee Members:

Prof. Dr. Yusuf Özyörük
Aerospace Engineering Dept., METU _____

Assoc. Prof. Dr. Oğuz Uzol
Aerospace Engineering Dept., METU _____

Prof. Dr. Ünver Kaynak
Mechanical Engineering Dept., TOBB _____

Assoc. Prof. Dr. Sinan Eyi
Aerospace Engineering Dept., METU _____

Asst. Prof. Dr. Ali Türker Kutay
Aerospace Engineering Dept., METU _____

Date: 05.02.2015

I hereby declare that all information in this document has been obtained and presented in accordance with academic rules and ethical conduct. I also declare that, as required by these rules and conduct, I have fully cited and referenced all material and results that are not original to this work.

Name, Last Name: Ezgi Anık

Signature:

ABSTRACT

EXPERIMENTAL INVESTIGATION OF THE EFFECTS OF TIP INJECTION ON THE CHARACTERISTICS OF THE TIP VORTEX ON A MODEL WIND TURBINE

Anık, Ezgi

M.S., Department of Aerospace Engineering

Supervisor: Assoc. Prof. Dr. Oğuz Uzol

February 2015, 74 pages

This study presents the results of an experimental study performed on a horizontal axis wind turbine to investigate the effects of spanwise steady tip injection on the tip flow characteristics of a model turbine. Experiments are performed in front of an open-jet wind tunnel facility on a specially designed model wind turbine that has a 3-bladed rotor with NREL S826 airfoil profile. The turbine has a specially designed injection system which consists of a pressure chamber, a hollow shaft, pressurized hub and blades with injection channels for tip injection. The model turbine is also instrumented with a torquemeter, a 6-axes Force-Moment transducer for load measurements, an electrical motor to control the rotational speed, a nacelle, a tower and a base. Time Resolved Particle Image Velocimetry (Tr-PIV) measurements are performed at 5 m/s constant wind speed, at TSR=5 for baseline and two selected injection ratios. Tr-PIV results showed that, injection changes the tip vortex as well as wake characteristics of the model turbine. Injection affects the size, location, vorticity and the trajectory of the tip vortex also; it causes an expansion in the wake and increases the velocity behind the turbine depending on injection ratio. In

addition, a power budget analysis is performed to see how feasible to use tip injection in sense of an active flow control method. To understand the relation between performance changes and tip flow field characteristics a 1D mass flow analysis is done. Results show that although tip injection has an increasing effect on performance characteristics of this model turbine it is mostly inefficient to use injection according to the power budget analysis. According to the mass flow analysis, tip injection increases the effective span therefore the mass flow rate which results in increase in performance characteristics dependent on injection ratio.

Keywords: Tip vortex characteristics, Active flow control, Tip Injection, Horizontal axis wind turbine

ÖZ

UÇ ENJEKSİYONUNUN UÇ GİRDABININ KARAKTERİSTİĞİ ÜZERİNDEKİ ETKİLERİNİN MODEL BİR RÜZGAR TÜRBİNİ ÜZERİNDE DENEYSEL OLARAK İNCELENMESİ

Anık, Ezgi
Yüksek Lisans, Havacılık ve Uzay Mühendisliği Bölümü
Tez yöneticisi: Doç. Dr. Oğuz Uzol

Şubat 2015, 74 sayfa

Bu çalışma kanat boyunca sürekli yapılan uç enjeksiyonunun, yatay eksenli bir rüzgar türbininin uç akış ve performans karakteristikleri üzerindeki etkilerini incelemektedir. Deneyler bir açık-jet kesitli rüzgar tüneli önünde ve özel olarak tasarlanmış model bir rüzgar türbini kullanılarak yapılmıştır. Model türbin, NREL S826 kanat profiline sahip üç palli bir rotora sahiptir. Uç enjeksiyonu için kullanılan sistem özel tasarlanmış ve bir basınçlı odaya, içi boş bir mile, basınçlı bir rotor göbeğine ve içinde uç enjeksiyonu için hava kanalları bulunan pallere sahiptir. Ayrıca model türbin yük ölçümleri için bir torkmetreye, altı eksenli yük-tork ölçere, devir kontrolü için bir elektrik motoruna nasel, kule ve bir temele sahiptir. Yüksek Hızlı Parçacık İmge Hızölçer (YH-PİH) deneyleri sabit 5 m/s rüzgar hızında, uç hız oranı 5 için referans ve iki farklı uç enjeksiyon oranında gerçekleştirilmiştir. PİH sonuçlarına göre uç enjeksiyonu model türbinin uç girdabının yanı sıra türbin iz

bölgesi karakteristiklerini de değiştirmektedir. Uç enjeksiyonu, uç girdabının boyut, konum, vortisite ve izlediği yolu etkilemekle beraber, türbin iz bölgesinin genişlemesine ve türbin iz bölgesindeki hızın artmasına neden olmaktadır. Ek olarak uç enjeksiyonun bir rüzgar türbininde aktif akış kontrol yöntemi olarak kullanılmasının ne kadar verimli olduğunu anlamak için güç verimliliği analizi ve de yük karakteristiklerinde meydana gelen değişimler ile uç bölgesinde meydana gelen akış değişiklikleri arasında bir bağlantı bulabilmek amacıyla kütle akış analizi yapılmıştır. Sonuçlara göre her ne kadar uç enjeksiyonu model türbinin güç/yük katsayılarında bir atışa sebep olsa da genel olarak verimsiz sonuçlar göstermiştir. Kütle akış analizine göre, uç enjeksiyonunun etkili kanat uzunluğunu arttırarak kütle akış miktarının artmasına yol açtığı böylece model türbinin güç/yük katsayılarını arttırdığı sonucuna varılmıştır.

Anahtar Kelimeler: Uç girdabı karakteristikleri, Aktif akış kontrolü, uç enjeksiyonu, Yatay eksenli rüzgar türbini

To my family because sun has all the answers…

ACKNOWLEDGEMENTS

I would like to thank my supervisor Dr. Uzol for his patience, guidance and helps during my graduate studies. I also want to thank my dear friend Senem Haser first of all for her brilliant idea that she brought us which ignites a very interesting project and for her help and friendship during my studies, I wish we could work with her until the end. Special thanks to Eda Doğan for her guidance and support during my freshman years. In addition, for their support I want to thank my project team Anas Abdulrahim, Bayram Mercan, Yashar Ostovan.

This study is supported by the Scientific and Technological Research Council of Turkey (TÜBITAK) under the project number 112M105 as well as by METU Center for Wind Energy (METUWIND). Their support is greatly appreciated.

I want to thank and give my deepest love to my dear family, my parents Filiz and Metin Anık, my beloved sister Burcu Anık Tolungüç, my dear and super brother in law Alp Tolungüç, my dear aunts Sema Yorgancı and Nur Acardağ and my grandmother Semiha Yorgancı, for their great support, love and belief in my work which enlightens my vision and encourages me to continue without hesitation.

And thanks to many that I cannot put their names but I will always be grateful for their existence in my life.

TABLE OF CONTENTS

LIST OF FIGURES

FIGURES

LIST OF TABLES

TABLES

NOMENCLATURE

AFC	Active Flow Control
CTA	Constant Temperature Anemometer
HAWT	Horizontal Axis Wind Turbine
NREL	National Renewable Energy Laboratory
PBC	Power Budget Calculation
PE	Power Efficiency
PFC	Passive Flow Control
TI	Turbulence intensity
A	Rotor cross sectional area [m^2]
$\mathbf{A_1}$	Rotor wake cross sectional area [m^2]
$\mathbf{C_P}$	Power Coefficient
$\mathbf{C_{PINJ}}$	Injection Power Coefficient
$\mathbf{C_{Pmax}}$	Maximum Power Coefficient
$\mathbf{C_T}$	Thrust Coefficient
$\dot{\mathbf{m}}$	Mass flow rate [kg/s]
$\mathbf{P_{wind}}$	Power available in the wind [Watt]
$\mathbf{P_{BL}}$	Rotor power for baseline case [Watt]
$\mathbf{P_{INJ}}$	Rotor power for injection case [Watt]
$\mathbf{P_{max}}$	Max rotor power according to Betz limit [Watt]
Re	Reynolds number
$\mathbf{R_M}$	Injection Momentum Ratio
$\mathbf{R_{TS}}$	Injection Tip Speed ratio
R	Radial distance [m]
ρ	Density of air [kg/m^3]
$\mathbf{U_\infty}$	Free stream velocity [m/s]

$\mathbf{U_{tip}}$	Velocity at the blade tip [m/s]
$\mathbf{U_{jet}}$	Mean velocity of Injected air [m/s]
$\mathbf{u_1}$	Rotor wake velocity [m/s]
$\mathbf{V_0}$	Far upstream velocity
T	Thrust force [N]
TSR,Ω	Tip Speed Ratio
x/R	Axial direction
y/R	Horizontal direction

CHAPTER 1

INTRODUCTION

As the world grows in population day by day, the energy need to keep the daily works to pursue therefore the consumption of the energy resources increases. Unfortunately the energy coming from the fossil fuels are diminishing rapidly. Besides, despite their high energy capacity, they are hazardous to the atmosphere and the environment that we are living in. In addition, other energy sources such as nuclear energy might be even more dangerous than fossil fuels. Therefore, need for clean, renewable and relatively endless energy sources increases. The large availability and ease of accessibility of the wind power draws the attentions more and more on itself. The idea of extracting the energy of the wind started to develop when the 20^{th} century was ending. In years, wind became a policy of the governments for local energy sources with the awareness of environmental pollution (Manwell, J. F., McGowan, & Rogers, A., 2009).Then, with increasing wind energy demand, wind farms become more and more widespread.

As the importance of a sustainable, renewable and clean energy need increases, the focus on efficiency on the wind turbines also increases. More efficient systems mean less demand on other energy sources. It is well known that every system interacting with the air is an area of interest of the aerodynamics since the efficiency of a wind turbine is highly dependent on its aerodynamic performance. Therefore this topic becomes an important concern of the researches.

Theoretically in an ideal case, a wind turbine produces maximum power if it can extract all the power of the wind passing through its rotor area given in equation 1.1, so all the kinetic energy in the wind converted into rotational kinetic energy on the rotor. However, in a real system this is not possible since it requires to wind speed goes to zero when it passes through the turbine rotor. According to the Betz limit, the maximum power a wind turbine can extract from the wind is limited in such a way that it is related with conservation of mass and energy through a wind stream around a wind turbine (Ragheb & Ragheb, 2011). This leads to a new theoretical power equation for wind turbines defined in equation 1.2, where C_{Pmax} ,is equal to 16/27=0.593, is defined as power coefficient which is the ratio between the actual maximum power extracted from the wind over the power available in the wind. According to the researches, today modern turbines can reach a maximum power coefficient which is quite close to 0.5 (Hansen, 2008). However, even with today's technology, it is not easy to reach wind turbine efficiency higher than 50%. This is due to the losses occurring in the system and the losses related to the aerodynamics are an important concern and it is under investigation for many years.

$$P_{Wind} = \frac{1}{2}\rho A U_{\infty}^{3} \qquad [1.1]$$

$$P_{max} = \frac{1}{2}\rho A U_{\infty}^{3} C_{pmax} \qquad [1.2]$$

Losses happening in a system are an inevitable part of the nature since every system in nature tends to preserve its current state. Therefore, any discontinuity or imbalance occurring in the system tried to be balanced by the system itself. For the wind turbines, one of the major aerodynamic loss mechanisms is the tip losses. Tip vortex which is a consequence of the tip losses is usually accepted as a source of loss mechanism for many other systems such as fixed wings, rotors and turbomachinery

flows. Simply it can be explained that, the boundary layer at the tip section of the airfoil tends to separate due to pressure difference (Duraisamy & Baeder, 2006). The cause of this separation occurs due to the discontinuity of a sharp ending wing or a blade tips. Wing tip vortices are generally appearing as a consequence of the lift generated by the wing which negatively affects the performance and aerodynamic characteristics of the wing itself. In more detail, the pressure difference between the wing surfaces causes a leakage at the tip which forms concentrated rotating structures, called as tip vortices, when it meets with the main flow at the wing tip. It is explained that the reason of the wing tip losses is the tip vortices caused by the pressure difference between upper and lower surface of the wing (Shen, Mikkelsen, Sørensen, & Bak, 2005),(Bai, Ma, & Ming, 2011) The tip vortex is not only a loss mechanism for its original source but also it is a loss mechanism for every system whichever its interacting with such as vortex-body interactions in rotorcrafts, turbomachinery blades and wind farms.

In recent year, tip vortices become a significant problem in sense of interaction of the tip vortices with the rotor of downstream turbines for successively arranged wind turbines in a wind farm. This issue causes performance losses therefore leads to a reduction in the total energy generation. In addition, noise created by these vortices causes noise pollution and negatively affects civilization around them (Hansen, 2008).

All these problems mentioned in aerospace fields can be reduced by controlling tip vortices with the help of some methods. In order to minimize as much as possible the negative effects of these vortices common approaches are usually focuses on preventing its formation or weakening the structure of strong vortices, increasing the dissipation rate or reducing their vorticity. In literature there exist many applications on the topic of controlling tip vortices. These methods are mainly classified as active and passive control methods. Passive methods are much more simplistic methods compared to the active ones since they generally introduce an extension, such as winglets, vortex diffusers and so on, to the wing itself and cannot be adjusted according to the changing flow conditions. The main reason of these is that passive

methods are usually designed and optimized for one selected flow condition. Despite their simplicity, passive control methods generally inadequate in terms of accommodate off-design conditions. Additionally, since passive methods require external structures, they also increase the weight and structural loads on the lifting surfaces. At this point, active control methods are introduced into the topic. Although active control methods are much more complicated systems compared to the passive methods, the capability of adjustment and fast response to changing flow conditions, active control methods are getting more and more attention in years. The most common active methods that are used to reduce the effects of tip vortices usually are tip blowing or suction from the wing tips, ejector nozzles, synthetic jets and plasma actuators and so on.

1.1. Literature Survey

1.1.1. Active Tip Vortex Control

Control of the tip vortices is a very important topic that is under investigation and becoming more and more popular among researchers. It is possible to achieve an increase in the aerodynamic performance of the fixed wings as well as increase in loads and moments of the control surfaces, rotor craft and turbomachinery blades and wind turbines by increasing the lift while decreasing the drag and noise with the help of control mechanism that are existed (Gursul, Vardaki, Margaris, & Wang, 2007). Many active control mechanism and their effects on tip vortices are examined. Some active control mechanisms are presented as mechanical systems simply have a moving solid surfaces for example "Gurney Flaps" moving along the wing span, active trailing edge tabs, or wing tip flaps, but they are complex and heavy systems compared to tip suction or blowing systems (Matalanis, Nelson, & Eaton, 2007), (Panagakos & Lee, 2006), (Greenblatt, 2012). It is showed that tip injection perpendicular or angular to the main flow is effective in terms of changing size, vorticity, turbulence levels, strength, core location, core structure and even the number of vortices shed from the tip (Margaris & Gursul, 2004). Another

experimental study on tip injection reveals that unsteady tip injection applied on low pressure turbine blades affects the size, core structure as well as wake size characteristics and reduces the pressure losses due to tip leakage (Mercan, Doğan, Ostovan, & Uzol, 2012).

Tip injection or tip blowing is a widely used active control method for rotary systems as turbomachinery and helicopter rotors. It is explained that, for turbomachinery flows, the gap between the turbine blades and the casing is the location of pressure distortion therefore location of where tip leakage formation occurs and causes of work and efficiency penalties (F. J. G. Heyes & Hodson, 1993). So, the control of the tip vortices and tip leakage is studied for turbomachinery cascades in sense of controlling tip leakage. Lu et al. studied steady tip injection in an axial compressor and showed that tip injection increased the operating range of the compressor and reduced the severe effects of the tip leakage vortex and also reduce the stalled mass flow rate amount by 7.69% (Lu, Chu, Zhu, & Tong, 2006). Nie et al. used steady micro air injection at the tip region of a compressor rotor and shows that injection may delay or prevent compressor stall by pushing the tip vortex towards downstream of the rotor (Nie, Tong, Geng, Zhu, & Huang, 2006). Geng et al. presented the effects of tip injection on a compressor rotor and showed that tip injection can modulate the leakage unsteadiness and stall characteristics (Geng, Zhang, Chen, & Huang, 2007). A waveform tip injection method is studied on a low pressure turbine cascade and a reduction in the pressure loss is observed up to 15% (Mercan et al., 2012).

Tip vortices play a very important role in terms of defining the aerodynamic and aeroacoustic characteristics of hovercraft rotors, especially for helicopter rotors. Previous studies performed on a hovering helicopter blade reveal that tip blowing is an effective method for controlling tip vortices. The study of Vasilescu shows that high pressurized jet blowing through the core of the tip vortex decreases the strength and the rotational speed of the vortex and increases its diffusion in the flow (Vasilescu, 2004). In his study, Han et al. drill channels from the leading edge through the tip chord of the rotor blades and make high pressurized air passage

through these channels and observed that during the hover, rotational speed of the tip vortices get reduced in an amount of 60% and the diffusion rate of them increased three times (Han & Leishman, 2004). Another active tip blowing method that has been used to reduce the effects of the tip vortices is synthetic jets generated by piezoelectric actuators. Numerical studies on synthetic jets that are placed at the upper surface of the helicopter blades shows that synthetic jets are able to reduce the tip vortex strength up to 14% (Liu, Sankar, & Hassan, 2000). In another study performed on hovering helicopter blades, Liu et al. showed that tip blowing from the upper surface of the blades is able to decrease the strength and increase the core size of the tip vortex similarly to a spoiler without causing any increase in power (Liu, Russell, & Sankar, 2001). However, it is shown that tip blowing from lower surface does exactly opposite effect compared to the upper side blowing and increases the tip loads, thrust, torque as well as strength of the tip vortex (Liu et al., 2001). In another study on synthetic jets, two different configurations for steady and unsteady cases are studied such as tangential blowing to the rotor blade and tip chord blowing from the center of the chordline in order to see the effects on the tip vortex. It is discovered that, blowing reduces the noise by reducing blade vortex interaction, reduces the strength of the tip vortex by disturbing the structure of the tip vortex and increases its diffusion. It is concluded that unsteady controlled blowing is more effective in terms of reducing the negative effects of the tip vortices and it can reduce the rotational velocity of the tip vortex up to 20% (Vasilescu, 2004).

1.1.2. Wind Turbine Tip Flow Control

Wind energy is one of the fastest developing energy sources due to being renewable and clean. Therefore it has an important place among energy sector. However, tip losses due to the tip vortices are reducing the efficiency of the wind turbines.

Many studies are conducted to increase the aerodynamic performance of the wind turbines. Special type V-shaped winglets called Mie-vanes are examined experimentally and numerically and it is found that they are effective in terms of

reducing the effects of tip vortices and they can increase the pressure coefficient of a wind turbine up to 15% (Shimizu, Imamura, Matsumura, & Maeda, 1995), (Shimizu et al., 1990). Furthermore, Shimizu et al. (2003) showed that, Mie-vanes are more effective on the aerodynamic performance of the wind turbines with relatively small aspect ratios (Shimizu, Ismaili, Kamada, & Maeda, 2003). Another passive control method that has been used on wind turbines to control the tip vortices is vortex diffuser which is a triangular extension that is placed on the pressure surface of the blades. Numerical studies show that vortex diffusers are capable of increasing the pressure coefficient and the efficiency of wind turbine and reducing the noise by reducing the effects of tip vortices (Bai et al., 2011). Studies done on winglets shows that winglets can increase the power generation of a wind turbine only around 2.77% dependent on winglet height, twist and incidence angle and also camber distribution (Johansen & Sørensen, 2006). When winglet and Mie-vane compared in terms of efficiency, it is found that Mie-vanes are more effective and provide more increase in wind turbine power coefficient. The main reason is that Mie-vanes generate a ring vortex in front of the wind turbine which increases the amount of mass flow rate passing through the wind turbine in addition to their mission of reducing effects of tip vortices which both have an increasing effect on the power coefficient. Furthermore, investigations show that there is no significant difference between using a winglet and increasing the blade span with the same amount of the winglet length on turbine aerodynamic performance of a wind turbine (Gaunaa & Johansen, 2007).

1.2. Objectives

There are two main objectives of this study: One is to examine is how different injection ratios affect the tip flow characteristics of the model wind turbine during its operation at a constant RPM and secondly how feasible to use tip injection as an active flow control method on a wind turbine in terms of flow power budget.

This thesis is consists of three main chapters which are explaining the work presented such as experimental procedure, results and conclusions.

In the Chapter 2, detailed experimental setup and procedure followed during the experiments are explained in detail. The experimental part presents the open-jet facility, model wind turbine and the experimental methodology.

Chapter 3 presents the results obtained from experiments performed at baseline and two different injection ratios for flow visualization measurements, instantaneous and mean flow measurement results around the tip region of the model turbine obtained from Tr-PIV as well as the hotwire and PIV measurement comparisons, the power budget calculations and mass flow analysis of the system.

In Chapter 4, the work presented will be summarized; related discussions and conclusions as well as future works to improve and enlarge the study will be presented accordingly.

CHAPTER 2

EXPERIMENTAL PROCEDURE

2.1. Wind Tunnel Facility

A specially designed and manufactured open-circuit open-jet wind tunnel facility, shown in Figure 2.1, is used in the experiments. Open-jet wind tunnel has a circular cross-section and it consists of an axial fan, a diffuser, a settling chamber and three flow straighteners to homogenize the flow and reduce the turbulence level as well as swirl created by the axial fan. Moreover, the open-jet exit is secured by a 3m x 3m x 3m cage in order to prevent any damage that might be happen during rotor testing. The tunnel is driven by a frequency controlled 45kW axial fan with 1.25 m diameter. The fan sucks the air from atmosphere and blows it through a 4.30 m long diffuser with 3 degrees of diffusion angle. After the diffuser, the flow comes to the first flow straightener, at the beginning of the 1.4 m long settling chamber, which is a coarse screen with open area ratio of 0.54. After 0.5 m downstream of the first screen, flow passes through a 10 mm thick honeycomb and after another 0.5 m straight section it goes through the second screen with open area ratio of 0.6. Finally, after travelling 0.4 m long last straight section, the jet flow meets with the atmosphere where the experiments are performed.

Before the experiments are performed, flow characteristics of the open-jet tunnel are measured at the exit plane for velocity and turbulence intensity distribution horizontally and vertically for selected motor frequencies. Additionally, the variation

of tunnel speed with respect to fan frequency characteristics also defined. According to the measurements, exit velocity and turbulence intensity distributions remain almost constant along the radius and the turbulence intensity levels are around 2.5% for every wind speed. The boundary layer thickness is measured as 7 mm from the wall of the jet exit. The velocity variation with tunnel frequency is found to be linear and the maximum jet-exit velocity measured is around 10 m/s. For more detailed information it can be referred to Anik et al. (2014) and Abdulrahim (2014) (Anik, Abdulrahim, Ostovan, Mercan, & Uzol, 2014) (Abdulrahim, 2014).

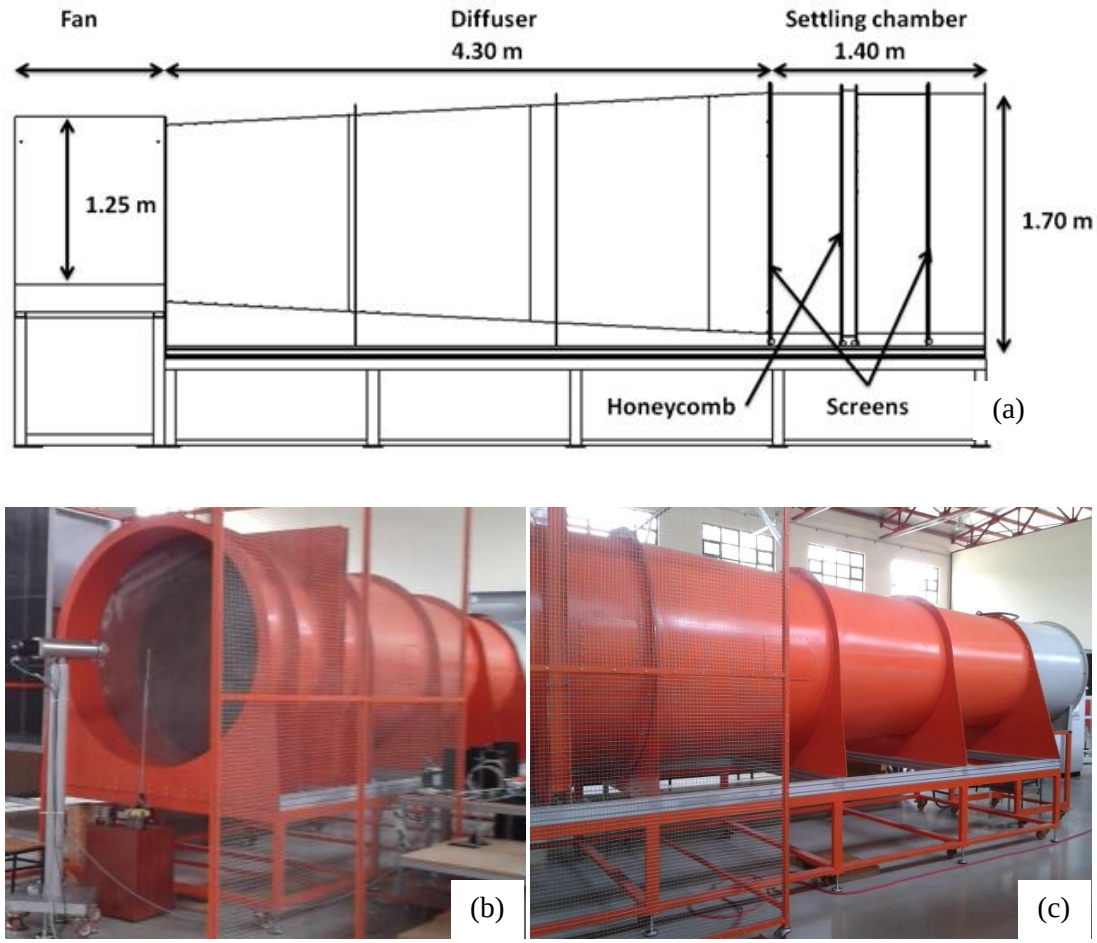

Figure 2. 1: Open-jet wind tunnel facility, (a) Tunnel dimensions, (b) and (c) Open-jet wind tunnel different views

2.2. Model Wind Turbine

Model wind turbine seen in Figure 2.2, is a horizontal axis wind turbine (HAWT) which is designed for the test purposes in a laboratory environment and also, it has a specially designed injection system which makes possible air injection from the blade tip during its operation. The model turbine consists of three main parts as rotor, nacelle and the tower which sits on a square base. Since the model turbine is

designed for the test purposes, in order to be able to keep the RPM therefore TSR constant, it is driven by 1.5 kW Panasonic AC servo motor of 4.3 N rated torque output and instrumented with HBM T20WN/5 Nm torque transducer and ATI six axes F/T transducer to determine the performance characteristics of the model turbine given in Figure 2.2 (c).

The tower of the model wind turbine is 1.524 m high and the total height of the turbine reaches about 1.815 m of height from the ground with its base. The nacelle part, which is 0.488 m long without rotor and the electrical motor, it has the main components and mechanical elements such as the motor, shaft, couplings, bearings and also some special parts such as pressure chamber for injection system and torquemeter for torque measurements. In addition a 6-axes Force/Torque transducer is placed between the nacelle and the tower in order to eliminate the drag created by the tower itself as seen from Figure 2.2.

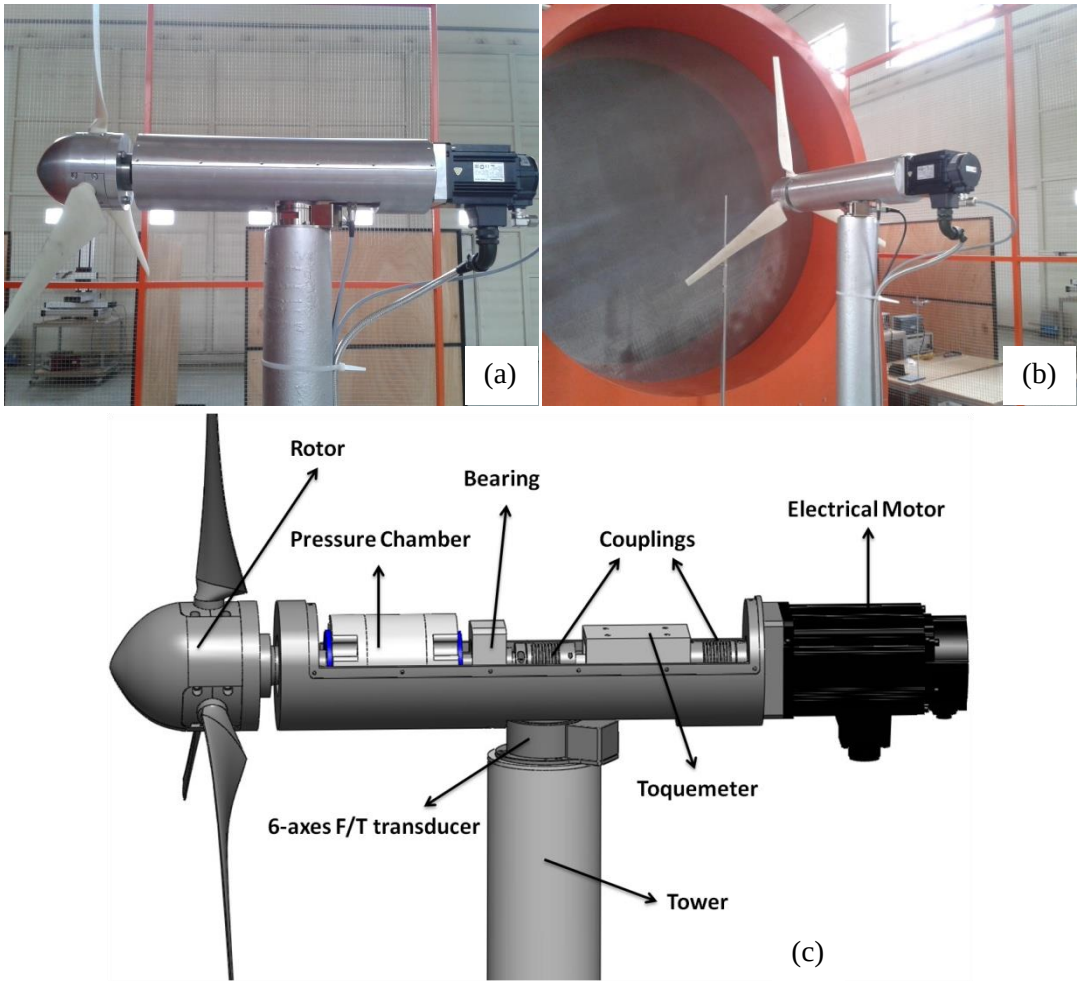

Figure 2. 2: Model wind turbine, (a) Side view, (b) isometric view, (c) CAD model and general layout

The model turbine has a three bladed rotor with 0.95 m diameter. The rotor geometry is a replica of the model wind turbine used in blind tests in NTNU by Adaramola and Krogstad (Adaramola & Krogstad, 2011). The rotor blades are non-linearly tapered and twisted along the span with 0.431 m long and the airfoil profile is NREL S826 given in Figure 2.3 which is designed as tip airfoil for wind turbines with a maximum thickness of 14% (Somers, 2005). Therefore the main purpose of selecting

this rotor configuration and airfoil geometry is to make possible of comparison the performance of the model turbine with another already existing model turbine and also to understand the tip flow field characteristics better.

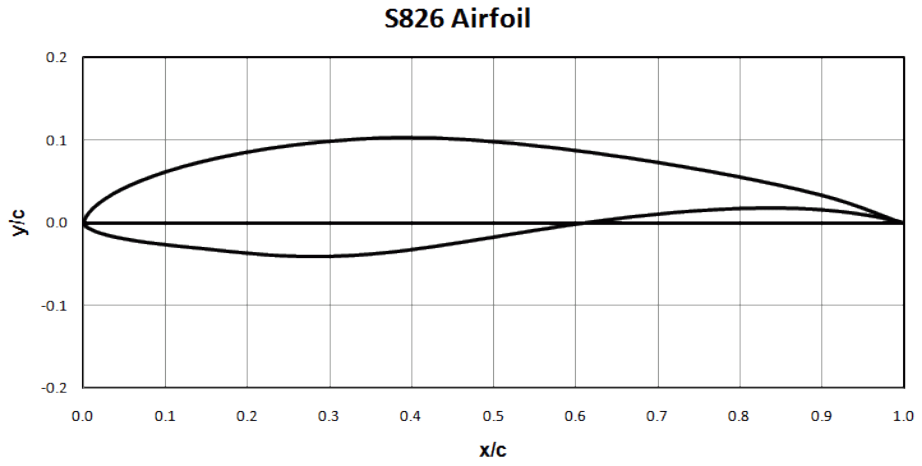

Figure 2. 3: NREL S826 airfoil profile (Somers, 2005)

The blades are manufactured with 3D printing technology from ABS plastic with ±0.6 mm precision. The Figure 2.4 gives the airfoil profile and the size and location of the injection slot at the tip chord. As it can be seen from the figure, the trailing edge of the blade is rounded to 0.6 mm diameter to be able to meet the manufacturing requirements. The injection slot which is located on the chordline of the tip section has a 6.50 mm long and 1.20 mm thick rectangular shape. The injection slot at the tip is placed where the tip airfoil has the thickest section and it

starts at 20% of the chord and it occupies 28.9% of the total chord length of the blade at the tip section.

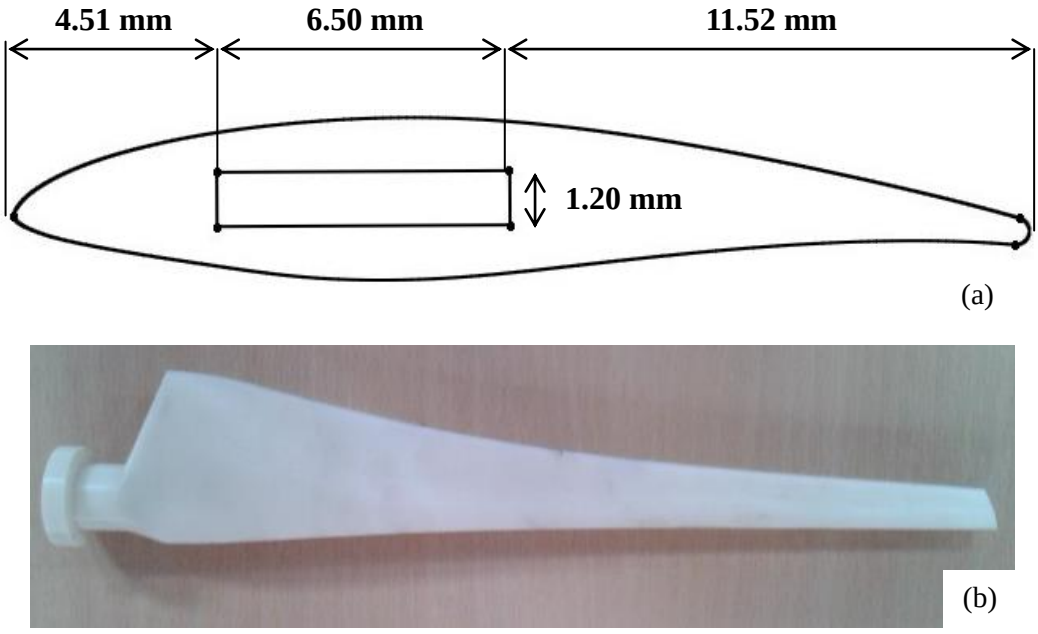

Figure 2. 4: (a) Blade tip geometry (b) 3D printed blade

2.3. Injection System

The major challenge in terms of the design of the model turbine was to find a proper way to transfer pressurized air from a stationary system, nacelle, to a rotational system, shaft, hub and the blades, for tip injection. This goal is achieved by a

specially designed pressure chamber which sits on a hollow shaft, a pressurized hub and blades with air channels inside which are presented in Figure 2.5. Pressure chamber contains mechanical seals to prevent air leakage and to allow rotation of the shaft. In addition, pressure chamber contains radial bearings in order to decrease the pressure on the shaft caused by its own weight. The shaft is consist of two parts; one part is solid and connected to the torquemeter, the other part is hollow and has holes on it to allow air transfer from the pressure chamber to the pressurized hub. All the connections, between shaft, pressure chamber, hub and the blades are also sealed with o-rings to eliminate any possible leakage in the system.

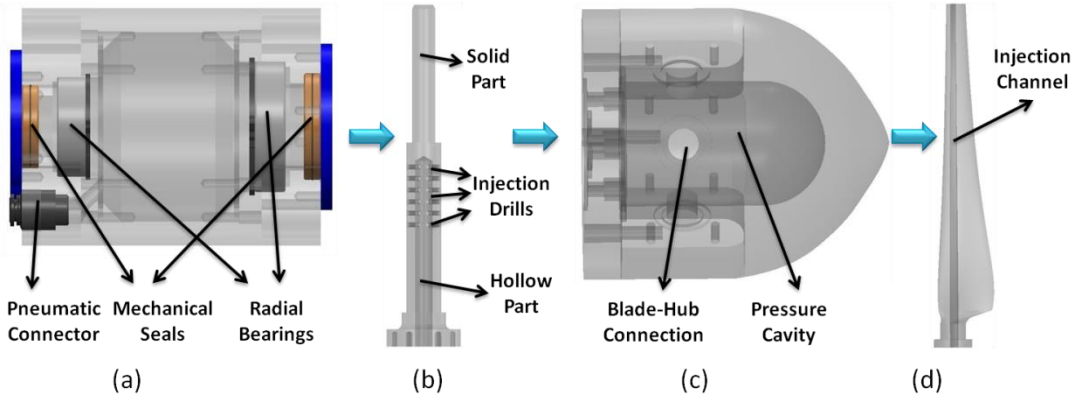

Figure 2. 5: 3D model of the injection system components in the order of the flow direction (a) Pressure chamber, (b) Shaft, (c) Pressurized hub, (d) Blade

The injection system is simple and effective and represented with two flow diagrams given in Figure 2.6 that shows the working principle of the system. The pressurized

air supplied by an external source comes to the pressure chamber with the help of a pipe which is connected to the pressure chamber via pneumatic connector, inside the pressure chamber, the compressed air goes through the holes on the hollow shaft while it's rotating, then it transferred to the pressurized hub. Finally, it passes to the injection channels lies in the blades from the hub-blade connections and get injected from the blade tips.

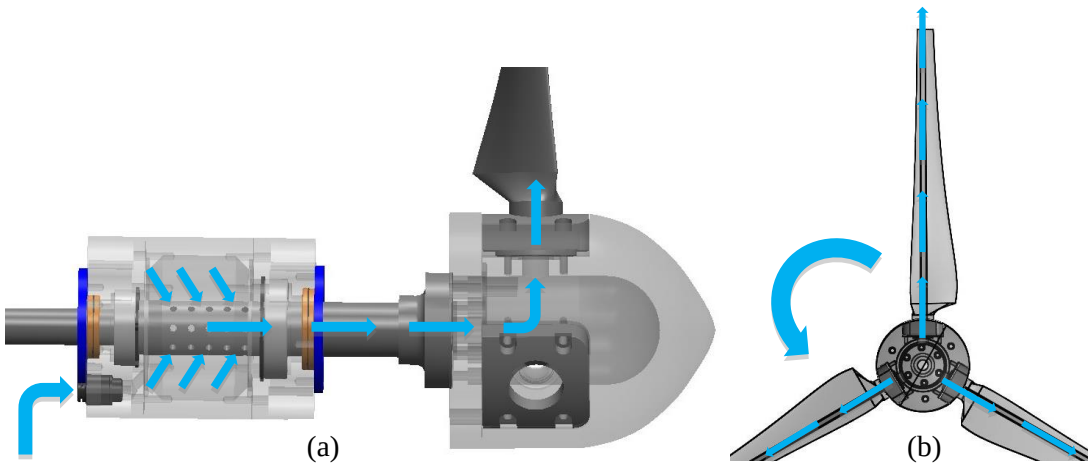

Figure 2. 6: Injection system flow diagram (a) Pressure chamber and pressurized hub parts, (b) Rotor part

2.4. Time Resolved Particle Image Velocimetry System

The PIV system used in the experiments is a time resolved system which has a 12 bit high speed camera with capability of operating at 2560 x 1600 pixels^2 (4 megapixel) resolution up to 1.5 kHz and a solid state high speed green Nd:YLF laser with 30mJ/pulse capacity. For the measurements, a 105 mm Nikkon-Nikkor Macro lens is used with aperture of 2.8. For the flow seeding, commercial fog fluid with medium density (glycol water mix) is used. For baseline and the maximum injection case, 1000 image pairs and for the minimum injection case 220 image pairs are taken for average flow field characteristics. 128x128 pixel^2 interrogation areas with 50% overlap are used during processing and the spatial resolution is 3.05 x 3.05 mm^2. The PIV setup and the components can be seen in Figure 2.7. A post processing method is used to eliminate the bad vectors and gaps in the data based on local vector validation called Gaussian global validation method.

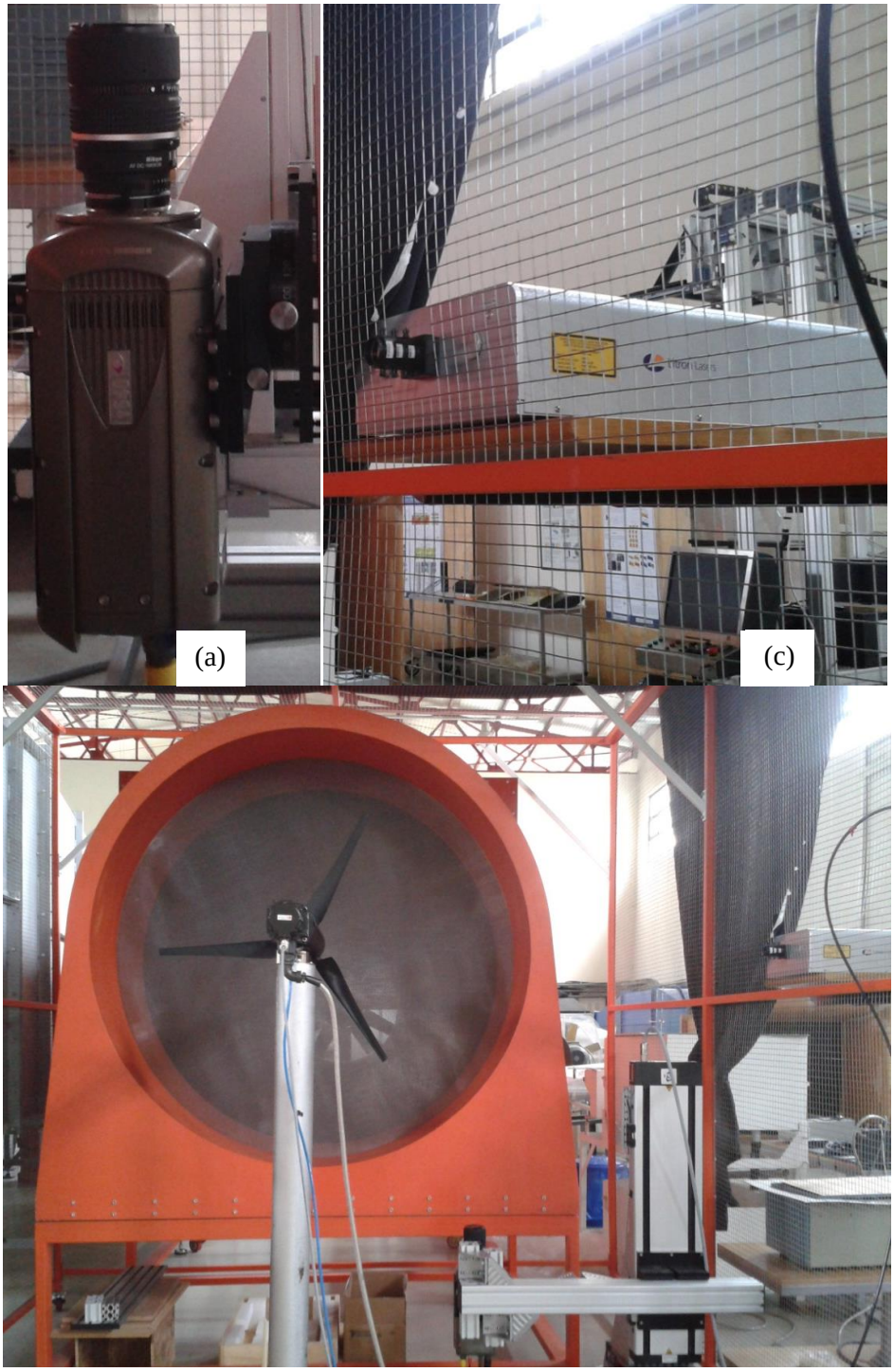

Figure 2. 7: PIV system components (a) Camera, (b) Laser, (c) Tr-PIV setup

2.5. Methodology

Measurements are performed at constant wind speed of 5 m/s and constant TSR value of 5 for baseline and two selected injection scenarios. The model wind turbine is placed 0.475 m away from the open-jet exit and the rotor plane is parallel to the jet exit plane. The rotor blades are mounted at zero pitch angle. The operating Reynolds number at tip chord is in order of 15000 and 46000 based on freestream velocity and the relative velocity at the tip respectively.

2.5.1. PIV measurements

Tr-PIV data is taken in a horizontal plane, corresponding to a radial plane, which crosses injection channel from the approximately midpoint at the tip section of the blades and it is perpendicular to the chordline (Figure 2.8).

PIV measurements are performed in a single window shown in Figure 2.8 which has a starting point at x/R=0.2 and y/R=0.9 and it is a 0.0761 x 0.115 m^2 rectangular area. The flow direction is from left to right and the rotation is out of the plane according to the measurement window figure. Experiments are conducted at Laser Pulse Repetition Rate (PRR) of 742 Hz, for Δt equal to 20 μs for each measurement conditions for 4 mega pixel resolution. The rotational data are collected in such a way that the data collection rate corresponds to 8 degrees angular displacement of the blades between two consecutive image pairs. For 1000 and 220 image pairs it equals to approximately 22 and 5 revolutions in total respectively. The mean values are calculated according to ensemble average of the collected data. Therefore, the mean data for baseline and maximum injection cases and for minimum injection case is the average of 22 and 5 revolutions of the rotor in total respectively.

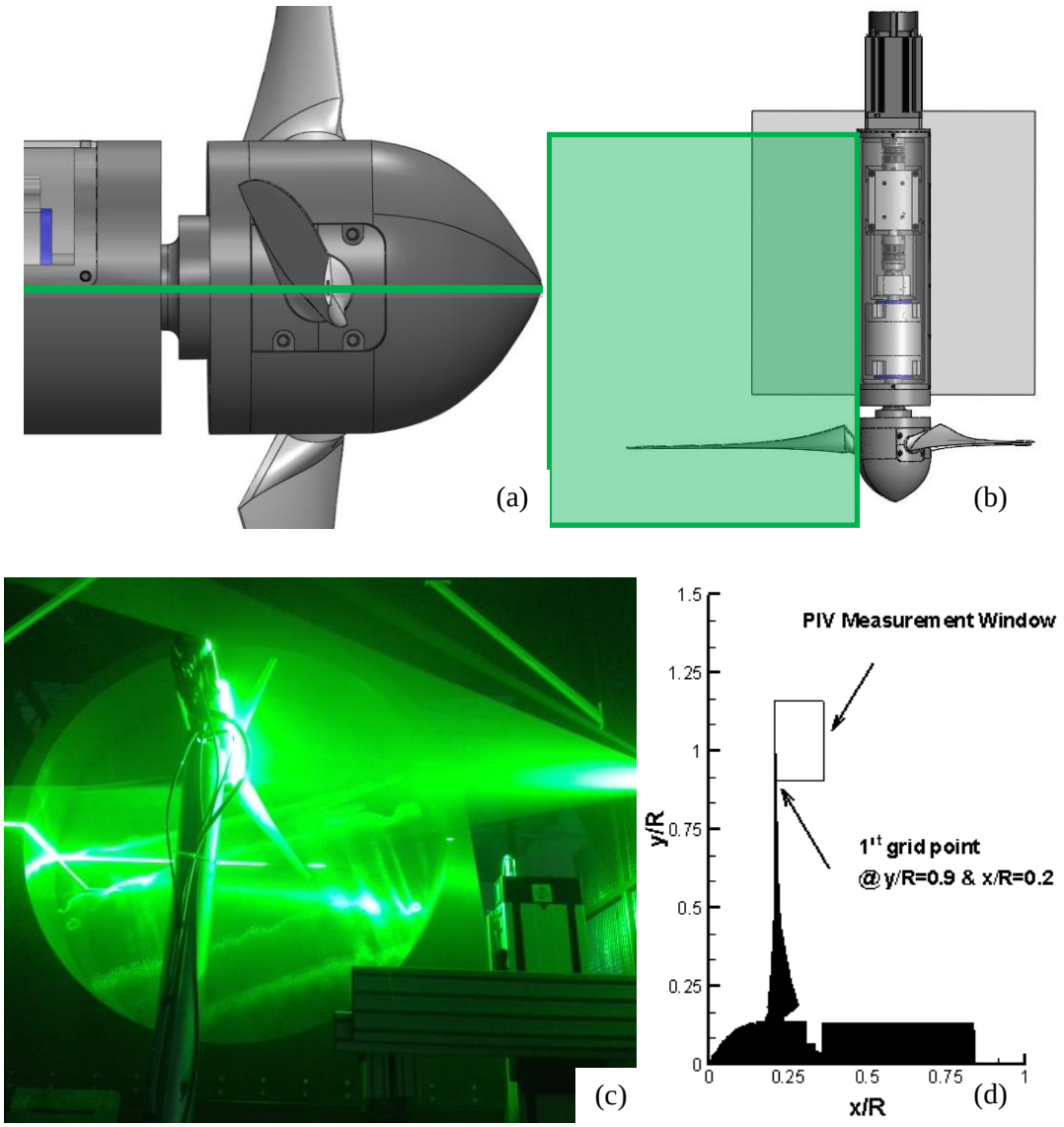

Figure 2. 8: PIV measurement plane details (a) Side view, (b) Top view, (c) PIV measurement setup, (d) PIV measurement window

2.5.2. Injection Cases

In order to obtain a realistic comparison with a real turbine for the PIV measurements, injection ratios are defined according to the tip speed. Therefore, the injection ratios as given in equation [2.1] are defined as the mean injected velocity from all blades over the tip speed of the rotor and the values are presented at Table 2.1. The main reason to not use this ratio for the load measurements is that injection ratio is changing with TSR value. So, to show a consistent ratio for each injection case, momentum ratio approach is used. Moreover, since PIV measurements are performed for one wind speed and one TSR value, it is more appropriate to use tip speed ratio.

R_{TS}= Injection Tip Speed Ratio

$$R_{TS} = \frac{U_{jet}}{\Omega R} \qquad [2.1]$$

Table 2. 1: Injection cases for tip speed ratios

Injection Case	**R_{TS}**
Case 1	1.16
Case 2	2.45
Case 3	3.26

For the power budget calculations given injection ratios are non-dimensionalized parameters according to the wind speed and defined as the total momentum rate of the injected air through the each blade over the momentum rate of the flow passing through the rotor disk in percentage as specified in equation [2.2]. Total injected air momentum calculated according to the jet flow velocity exiting each blade using a pitot-tube. According to the calculations the injection ratios according to the freestream velocity are given in Table 2.2. For more information it can be referred to Abdulrahim (Abdulrahim, 2014).

R_M= Injection Momentum Ratio

$$R_M = \frac{\sum \dot{m}_{jetn} U_{jetn}}{\dot{m}_{rotor} U_\infty} \qquad [2.2]$$

Table 2. 2: Injection cases for momentum ratios

Injection Case	R_M at 5 m/s	R_M at 6 m/s
Case 1	0.20%	0.10%
Case 2	0.70%	0.50%
Case 3	1.30%	0.90%

2.6. Uncertainty Estimations

The uncertainties and measurement errors that occur during the experiments are estimated according to the capabilities of the measurement devices, the variations in the measured data as well as human errors. The variation in tunnel speed is monitored before the experiments and it is estimated less than 0.8%. Before each experiment, the tunnel is left running so the flow can develop and reach to a steady level. For the PIV measurements, the error mostly comes from PIV cross-correlation algorithm and also from averaging. The accuracy of the cross-correlation algorithm is shown as less than 1% for a particle move within 5 to 10 pixels as explained (Mercan, 2012). According to Uzol et al. (2007) for an average field calculation the statistical error converges after 100 image pairs, therefore all the PIV averages are considered enough for the average field representations (Uzol, Brzozowski, Chow, Katz, & Meneveau, 2007).

CHAPTER 3

RESULTS

This chapter presents the results obtained from Tr-PIV measurement of tip flow field characteristics of the model wind turbine, at baseline and two different injection scenarios which consists of flow visualization, instantaneous and mean flow characteristics as well as PIV and hotwire measurement comparison and power budget and 1D mass flow analysis.

3.1. Flow Visualization

In this section, tip flow characteristics of the model turbine with and without injection are examined.

Flow visualization study is performed by using instantaneous raw images taken with the PIV system. The pictures cover the tip area of the blade and represent the flow behavior around the tip with and without injection. The main focus of the flow visualization is to observe the general structure and characteristics of the tip vortex. In Figures 3.1 to 3.3 the images are selected at a time where the blade crosses the laser sheet and the tip vortex is shed. The difference between the angular positions of the blade for successively selected raw images is 8°.

Figure 3.1 shows the visualization of the tip vortex for baseline condition. It is well known that a vortex is created due to leakage, and then shed from the blade tip. One can notice that, tip vortex starts with a small concentrated core size at the same level of the tip section and then it covers a slowly enlarging path with increasing core size along the wake region. The tip vortex endures through the measurement area and does not dissipate in the flow. Figure 3.1f is the superimposed image of five consecutive images taken with PIV to better visualize the path of the tip vortex and the expansion of the wake region downstream of the turbine rotor. A secondary blurry vortex core that is visible in the images is a ghost image of the second frame of the PIV image pair. This phenomenon sometimes occur due to the data leakage between two frames during the image capturing process However, it does not affect the analysis during the image processing since it is a false image.

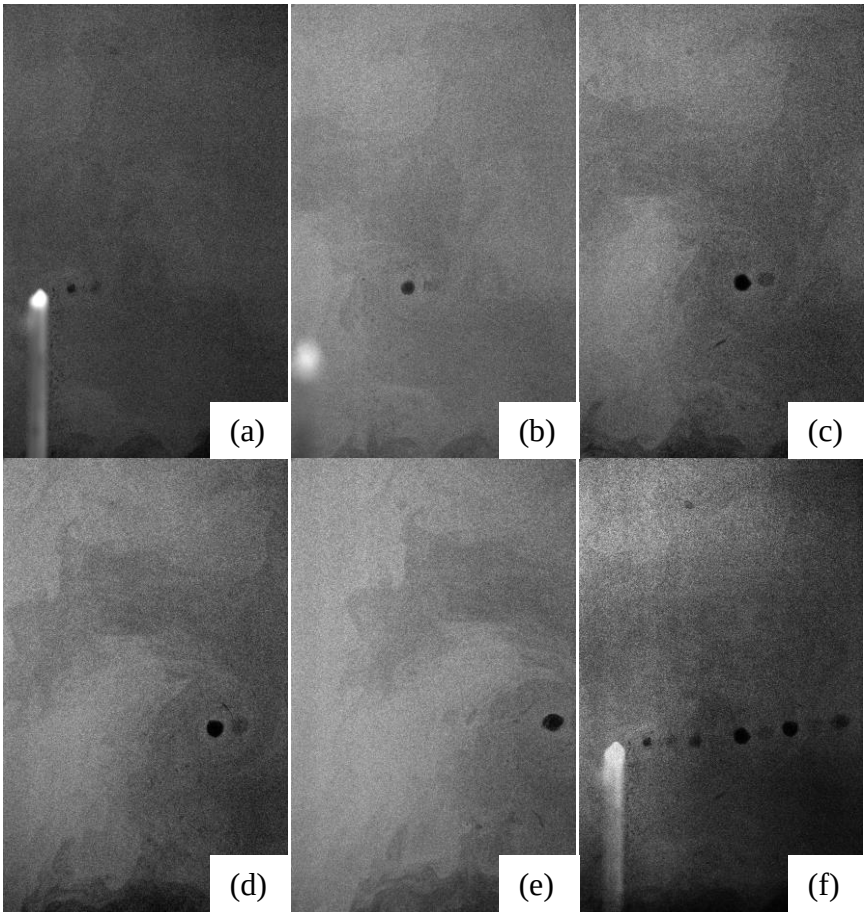

Figure 3. 1: Flow visualization for baseline case. (a) to (e) Raw images. (f) Superimposed image.

In Figure 3.2, images represents the tip flow under the effect of minimum injection case of R_{TS}=1.16. At the first sight, it can be seen that, there is a no clear evidence of a concentrated tip vortex as found in the baseline case such as a dark core region but still there is a vortex structure that can be distinguished in Figure 3.2a. The tip vortex in this case seems to have a larger core, relatively, it is less concentrated and also the core center is displaced further away from the blade tip. The streamwise trajectory of this vortex seems to be pushed radially outwards causing an enlarged wake boundary

downstream of the turbine due to injection. Another point to note is that the vortex seems to dissipate and mix with the main flow much quicker compared to the vortex structure captured at baseline case in the PIV measurement region.

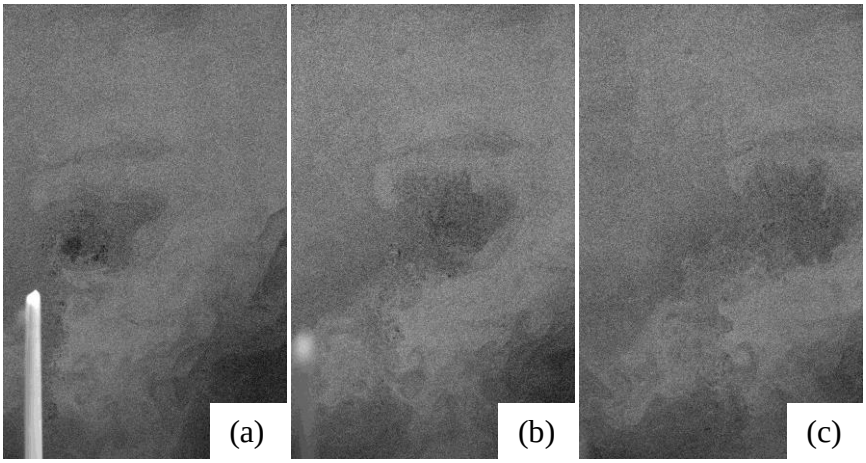

Figure 3. 2: (a) to (c) Flow visualization for injection case R_{TS}=1.16

Figure 3.3 shows the results of flow visualization for the maximum injection case defined as R_{TS}=3.26. One can directly notice the strong jet flow exiting from the blade tip. Due to the strong jet injection the wake boundary is pushed further away from the blade tip compared to other two cases. There is no evidence of the tip vortex structure in the raw images. On the other hand, if examined carefully, it seems to there is a vortex pair at the upper right corner of Figure 3.3c. This is most probably

the counter-rotating vortex pair formed as a consequence of the strong jet flow mixing with the main stream.

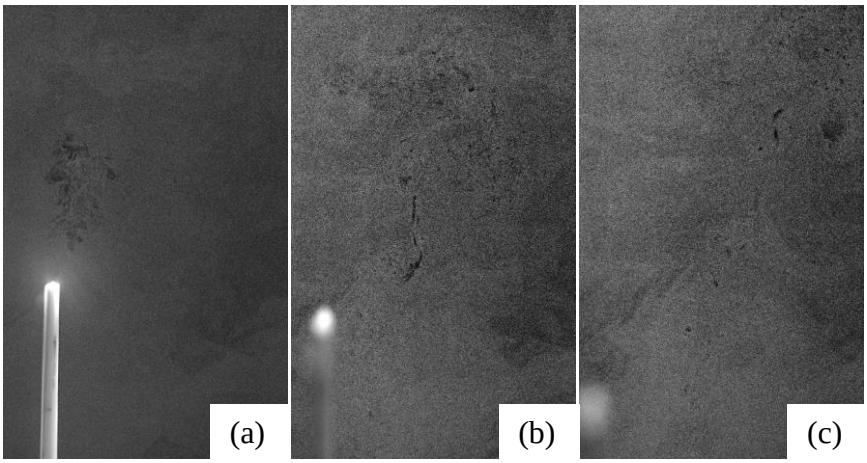

Figure 3. 3: (a) to (c) Flow visualization for injection case R_{TS}=3.26

3.2. Analysis Results

In this section PIV analysis results are presented to give a better insight of the tip flow characteristics. Results obtained from the PIV measurements are presented under two main sections as the instantaneous flow fields and mean flow fields for velocity, vorticity, turbulent kinetic energy and flow angle distributions to show what is happening with and without injection at the tip flow and also, how different injection ratios effect the characteristics of the tip flow during the operation of a

model wind turbine. The measurements for the tip flow field are performed at 5 m/s wind speed and at TSR=5 for baseline and two different injection scenarios for R_{TS}=1.16 and R_{TS}=3.26.

3.2.1. Instantaneous Flow Field

The instantaneous flow field shown in this study represents the time after the blade just passes through the laser sheet. The data contains the information about the behavior of the tip vortex for baseline and injection cases of R_{TS}=1.16 and R_{TS}=3.26. Similar to the flow visualization part, the instantaneous flow field contour plots are represented in a sequence where the difference between the angular positions of the blade for successively selected raw images is 8°.

3.2.1.1. Velocity Field

In Figure 3.4, the instantaneous velocity filed for baseline and two injection cases are represented. The first column in the figure represents the baseline case for four successive instantaneous flow fields taken just after the tip vortex shed from the blade tips. In the baseline case, the formation of the tip vortex and the wake can be observed quite clearly. The evidence of tip vortex can be understood from its core region where the velocity in the core is very slow and almost equal to zero which is marked as blue region in the Figure 3.4. This is due to the circular gap at the vortex center which is also captured in flow visualization part. This tip vortex shed from the blade tips moves with the wake at the rotor tip with a slowly expanding pattern as it is expected. When it is looked at the injection case of R_{TS}=1.16, the flow patterns are quite similar compared to the baseline case with some very slight differences. The tip vortex seen in the baseline case has a strong trace in the wake in terms of a more concentrated structure and a very distinctive core region and it does not disappear within area of investigation. On the other hand, the vortex found in the injection case of R_{TS}=1.16, has a diminishing trace and it seems to disappear in the wake slowly. Moreover, there is also a small difference between the location of the vortices found in baseline and injection case of R_{TS}=1.16. The tip vortex at the baseline case is

more dominant and appears to be on the wake boundary while the vortex fond in injection case of R_{TS}=1.16 is found to be more sunk in the wake region. The biggest change happens at the injection case of R_{TS}=3.26. If we look at the maximum injection, we see an entirely different flow field. On the contrary to the baseline and injection case of R_{TS}=1.16, a dominant jet flow and an additional vortex pair trace is discovered. Also, unlike the other two cases, the shape and the expansion characteristics of the wake domain changes dramatically. There can be seen a sudden expansion of the wake boundary due to high velocity of the jet flow coming out of the blade tips.

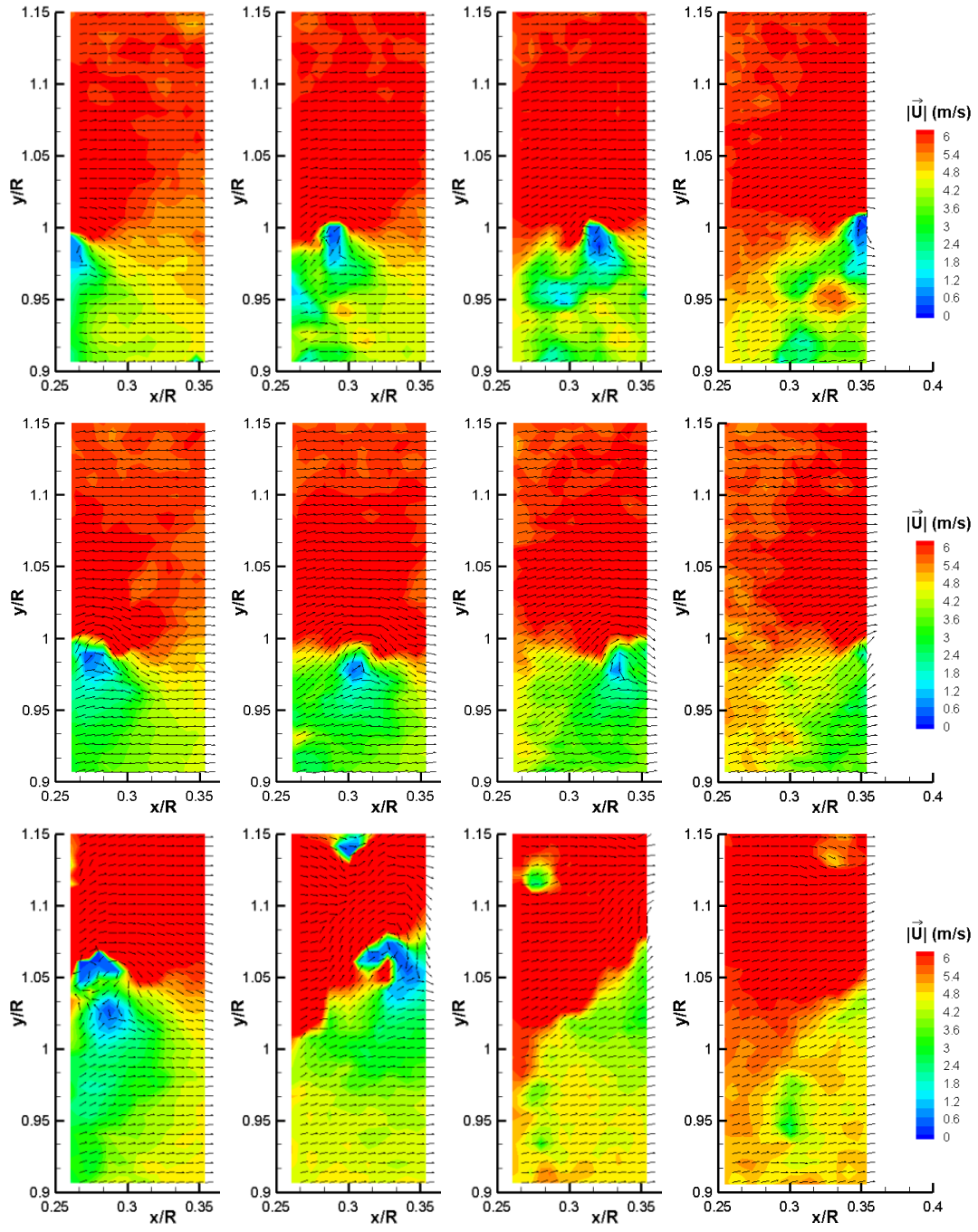

Figure 3. 4: Instantaneous velocity field, *1st row*: Baseline case, *2nd row*: Injection case for R_{TS}=1.16, *3rd row*: Injection case for R_{TS}=3.26

3.2.1.2. Vorticity Field

Instantaneous vorticity field given in Figure 3.5 shows the tip vortex evaluation with and without injection. The baseline case given in the first column, the usual behavior of the tip vortex following the wake boundary can be seen explicitly. It can be seen that a concentrated vortex at the tip forms and moves along wake boundary. Although, there is no significant difference seen for the velocity field between baseline and injection case of R_{TS}=1.16 there is a difference for the vorticity field in terms of vortex size and location. The major difference is the size, location and the vorticity of the tip vortex. There is an enlargement of the tip vortex despite the expectation of a smaller vortex structure seen in the velocity filed. Also, the shape of this vortex seems to have more irregular form compared to the tip vortex captured at the baseline case. Heyes and Smith shows that, blowing causes an extra mass flow introduction in the vortex therefore the core size and growth rate of the tip vortex can be increased depending on blowing rate (A. L. Heyes & Smith, 2004). In addition, another vortex structure shows up with smaller size and with opposite rotational direction at the upper side of the main vortex. This counter rotating vortex might be appearing due to jet flow introduced into the flow with tip injection. If we look at the injection case of R_{TS}=3.26, as similar to the velocity field, a counter rotating vortex pair dominates the flow instead of tip vortex. This is a well known phenomenon that when a jet flow meets with a stagnation or relatively low velocity flows, a counter rotating vortex pairs appear at the boundaries of the jet flow (Duraisamy & Baeder, 2006), (Ostovan, 2011). In addition, Margaris and Gursul (2004) also showed that, the number of the secondary vortices formed is proportional with the number of jets introduced into the flow moreover, as the blowing rate and number of jets increase, tip vortex moves away from the tip and become more weak (Margaris & Gursul, 2004). Beside the dominant counter rotating vortex pair, a structure very similar to the tip vortex appears under the dominant vortex pair with smallest size and more weakened compared to the baseline and minimum injection case.

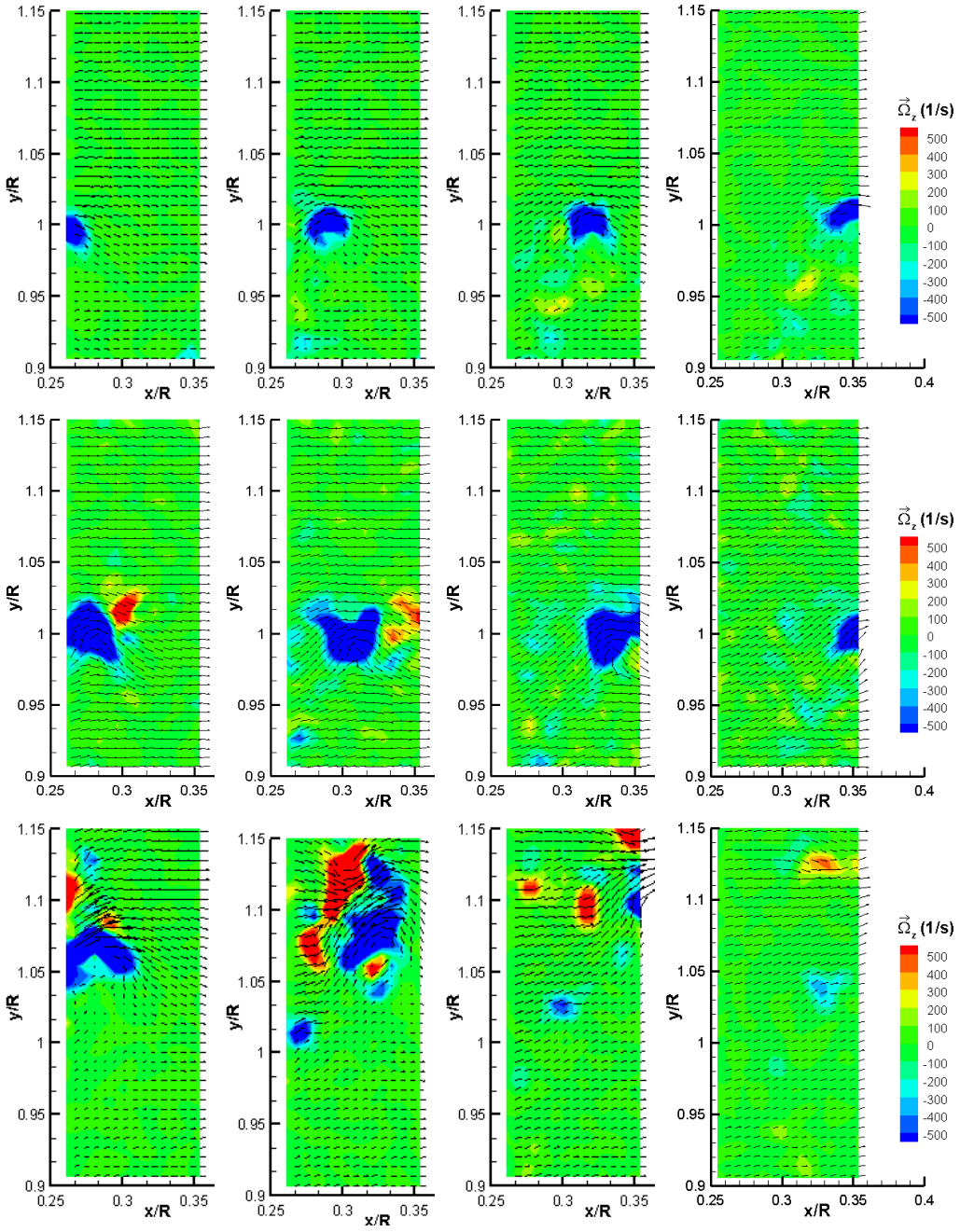

Figure 3. 5: Instantaneous vorticity field, *1st row*: Baseline case, *2nd row*: Injection case for R_{TS}=1.16, *3rd row*: Injection case for R_{TS}=3.26

3.2.2. Mean Flow Field

The mean flow field given in this study shows the tip flow evaluation with increasing injection rate. Results are shown in this section represents the baseline and injection cases of R_{TS}=1.16 and R_{TS}=3.26 for mean axial velocity, mean radial velocity, mean velocity magnitude, mean vorticity, turbulent kinetic energy, and flow angles fields.

3.2.2.1. Velocity Field

The 2D velocity field obtained from PIV measurements are presented as mean axial, mean radial and mean velocity magnitude field in this section.

When we look at the mean axial velocity contour plots given in Figure 3.6, gradually changing flow field characteristics at the tip of the rotor blade with injection can be seen. There are three major changes can be found in contour plots. First of all, it is clear that as injection ratio increases, the wake boundary gets pushed away from the rotor tip and becomes thicker. When it is compared with the baseline case, the shape of the wake boundary does not change but only get pushed radially outward for the injection ratio of R_{TS}=1.16. The greater change occurs to the wake characteristics behind the rotor for the injection case of R_{TS}=3.26, as both wake shape and thickness change dramatically. Secondly, an intermediate region is introduced with the injection to the flow and this region becomes more effective as the injection ratio increases and finally starts to dominate the flow for the highest injection ratio case. Finally, the velocity variation behind the rotor changes with injection. Although the velocity levels behind the rotor seems similar for baseline and R_{TS}=1.16 cases, in case of the maximum injection ratio, the velocity in the wake region visibly increases.

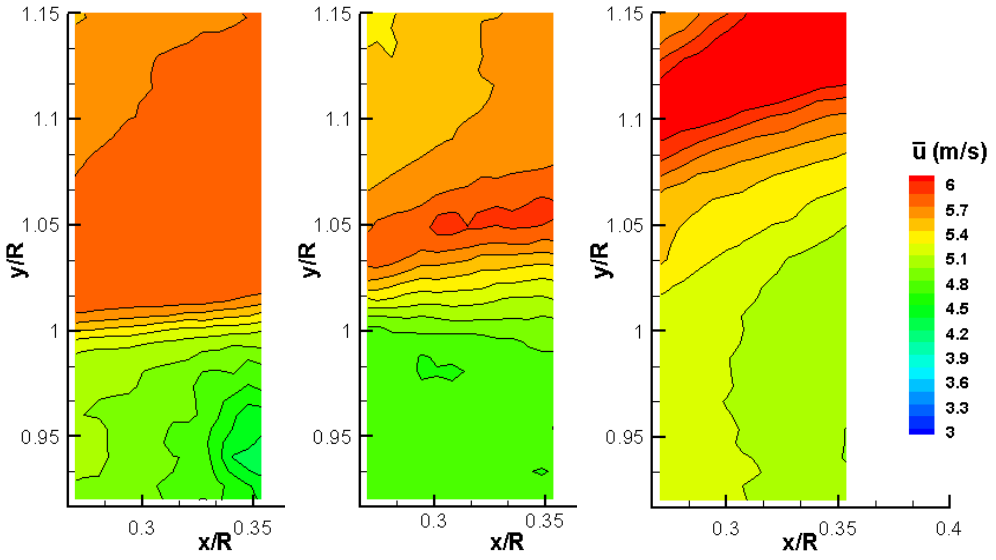

Figure 3. 6: Mean axial velocity field comparison, *from left to right*: Baseline, R_{TS}=1.16 and R_{TS}=3.26

Line comparison of the normalized velocity variation according to the freestream velocity is performed at x/R=0.31 location. The effects of different injection scenarios is given in Figure 3.7, on the mean axial velocity field behind the rotor, It can be said that in general, the velocity magnitude behavior along the spanwise direction has three major regions such as constant region before tip, velocity increase region and velocity recovery region. For y/R is smaller than 1, all variations show almost constant behavior along the span. Near the tip region (y/R~1), there is a dramatic change in mean axial velocity for baseline and injection case of R_{TS}=1.16 while the maximum injection case is kept constant up to y/R=1.05. It can be seen that injection case of R_{TS}=1.16 shows similar trend with baseline case in terms of velocity change near the tip region however with a shift in maximum velocity magnitude location in radial direction. When we look at the maximum injection case, it shows a similar yet smoother change compared to the other two cases. After the velocity reaches its maximum value for all three cases, the velocity away from the tip region starts to recover to the freestream velocity as expected. For baseline case, the

velocity recovery occurs right after the tip region while for injection cases it occurs at a farther distance after a velocity peak is reached due to injection. The velocity recovery starts after the jet region as it can be seen for injection case of R_{TS}=1.16. For injection case of R_{TS}=3.26, due to the restriction of the measurement plane, only the velocity peak region is captured partially at this axial location and after some distance a velocity recovery region is expected for this case similar to the baseline and minimum injection cases. In addition, as it is mentioned previously, the velocity levels behind the rotor are higher for R_{TS}=3.26 case while the baseline and R_{TS}=1.16 cases shows very close variations.

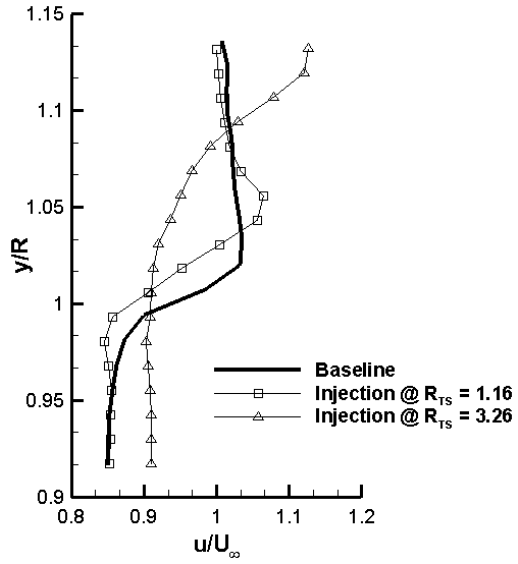

Figure 3. 7: Normalized mean axial velocity field comparison at x/R=0.31

Tip flow of a wind turbine is highly three dimensional due to the rotation and presence of the tip vortex. The tip vortex is a structure defined in axial, radial and

tangential directions (Micallef, Akay, Sant, Ferreira, & Van Bussel, 2011), therefore the flow around the tip should have radial components especially near the blade. In addition, spanwise injection also contributes to the radial velocity component near the tip section. Although it is small compared to the axial velocity, for baseline case there is two relatively high radial velocity regions exist where one is very close to the blade and concentrated along the span which is mostly due to the rotational motion and one goes along the wake boundary where the tip vortices are dominant (Figure 3.8). A similar pattern is seen yet with higher radial components in injection case of R_{TS}=1.16. Due to the jet velocity exiting from the blade tips, there is a concentrated radial motion captured at the tip section. Similar to the findings from previous sections, for the R_{TS}=1.16, the radial velocity region caused by the tip vortices occurs at a farther spanwise location with higher radial velocity magnitude compared to the baseline case. For the maximum injection case of R_{TS}=3.26, one can see that there is a very saturated radial velocity region where the injected jet dominates the flow and also creates relatively high radial velocity region along the blade span. Different from the baseline and minimum injection cases, the high radial velocity region goes along the wake for the maximum injection case.

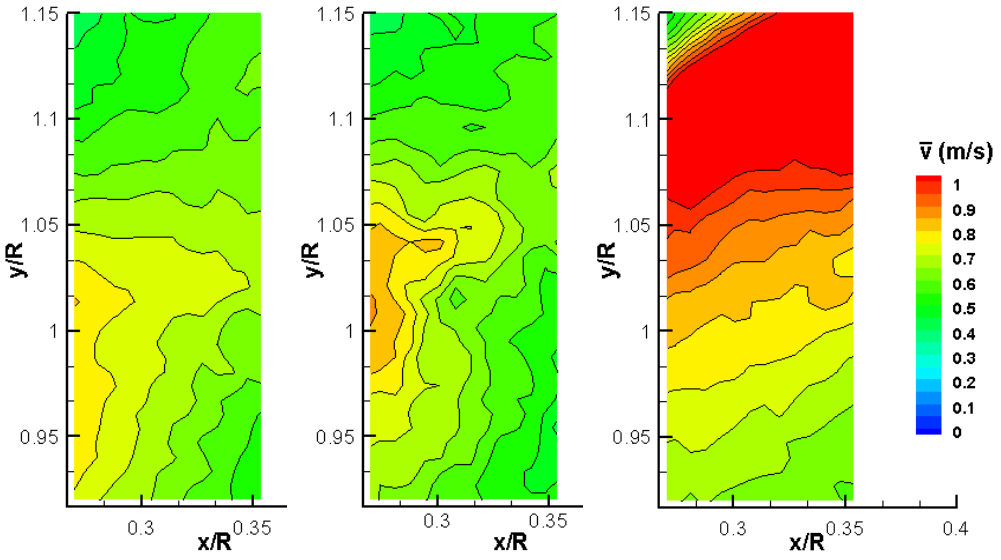

Figure 3. 8: Mean radial velocity field comparison, *from left to right*: Baseline, R_{TS}=1.16 and R_{TS}=3.26

The effects of injection can be seen more clearly from Figure 3.9 where the line plots are represented at an axial location of x/R=0.31. The radial motion observed for baseline case at this location shows an increasing pattern up to y/R=1.02 where the vortex boundary occurs and then starts to decrease. For the R_{TS}=1.16 case, it is seen that there is a double velocity peak region occurs after the blade tip. This effect is also visible in contour plots where there is a concentrated region around x/R=0.31 location. This region is mostly occurs due to the enlarged and disturbed vortex structure found in instantaneous vorticity field for this injection scenario. If we look at the R_{TS}=3.26, a similar pattern with magnified velocity levels exists of the radial velocity with a high peak region. As it is clear, after the velocity peak, the values start to decrease and they are expected to reach to the main flow levels.

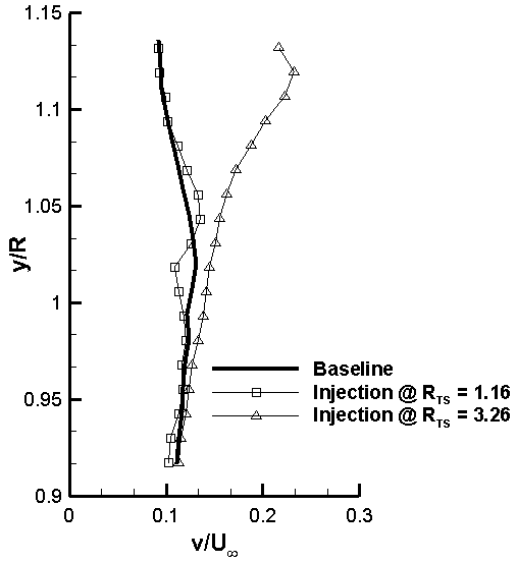

Figure 3. 9: Normalized mean radial velocity field comparison at x/R=0.31

To present the tip flow field characteristics better, mean velocity magnitude field is given in Figure 3.10. It can be seen that the mean velocity magnitude contours are quite similar to the mean axial velocity magnitude contours as expected since the main flow is in axial direction around the wind turbine and the biggest changes occur in axial direction. Therefore it can be said that the major impact of the injection occurs in axial direction as expected.

Similar to the axial flow characteristics, there is a significant change in wake characteristics around the rotor tips. The expansion and the shape of the wake boundary characteristics changes entirely when injection ratio of R_{TS}=3.26 is applied. The wake expansion characteristics for the baseline and the R_{TS}=1.16 are quite similar while the characteristics for R_{TS}=3.26 case changes dramatically. Heyes and Smith (2004) showed that, the wake trajectory can be changed depending on the jet angle (A. L. Heyes & Smith, 2004). For R_{TS}=3.26, if we consider that the exiting jet is in radial direction and the main flow is in axial direction, it is expected that a

dramatic change occurring at the wake shape. Secondly, the velocity behind the wake is increases with increasing injection rate. When it is examined the velocity contours in the wake region, there is a significant increase for the maximum injection ratio case. Additionally, according to the result obtained from the mean velocity field, there is an additional flow region occurs with injection due to the jet flow introduction to the flow. At the minimum injection case, the jet flow is relatively weak and follows the freestream flow. On the other hand, at the maximum injection ratio, jet flow dominates the main flow affecting wake characteristics. Finally, when we look at the contour around the tip region, it can be found that with injection, contour lines become wider and more spread and expanding along the wake unlike the baseline case where contours are more concentrated and regular near the tip. In addition number of contour lines increases with the presence of the tip injection which creates a smoother passage between wake region and the freestream flow.

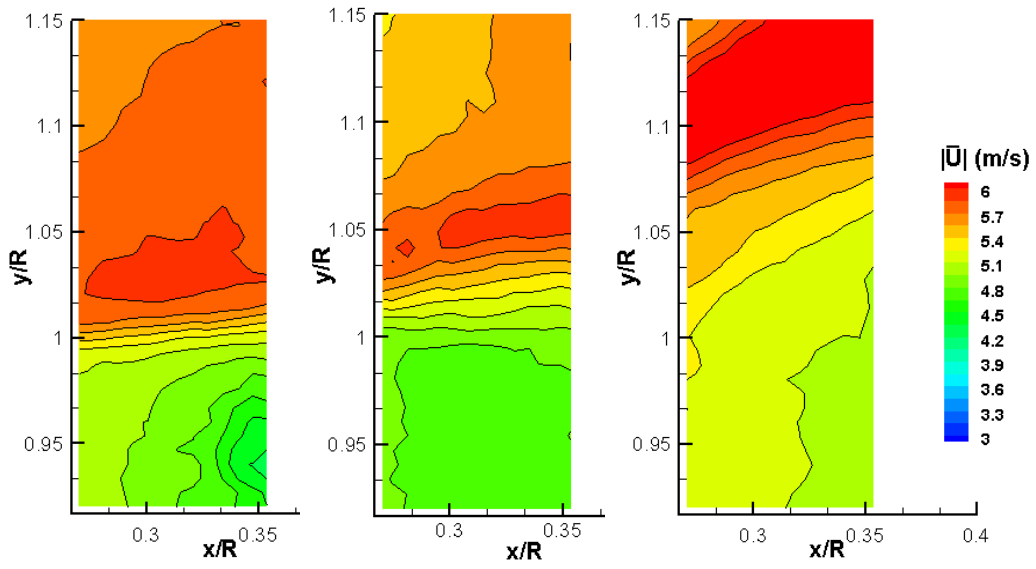

Figure 3. 10: Mean velocity magnitude field comparison, *from left to right*: Baseline, R_{TS}=1.16 and R_{TS}=3.26

The variation of the mean velocity magnitude field behind the rotor is presented as normalized similar to previous cases for line comparison at x/R=0.31 (Figure 3.11). The results obtained are in a good agreement and very similar to the results shown in mean axial velocity distributions. There is a three specific region as wake, tip velocity increase and recovery region in general. One can notice that as it is seen in axial variation there is an increase in velocity magnitude before the blade tip section for injection at R_{TS}=3.26 compared to the baseline and injection case of R_{TS}=1.16. One possible reason is that injection decreases the velocity deficit behind the rotor. According to study performed by Mercan (2012) for different injection scenarios on a low pressure turbine cascade, injection has a decreasing effect on velocity deficit after 95% span location (Mercan, 2012). Minimum injection case and baseline case shows very similar behavior behind the rotor as well as at the region away from the tip section. The reason can be the ratio of the injection for the R_{TS}=1.16 case. The amount of injected air and the injected air velocity is very small compared to the maximum injection case. Therefore, in that injection case, the characteristics behind the wake in terms of velocity deficit may not be get affected significantly as expected. Moreover, it is seen that the velocity away from the rotor tip starts to recover to the freestream velocity for the baseline and R_{TS}=1.16 cases.

It is understood that with injection the effective span increases. In literature it is proven that spanwise tip injection or tip blowing increases the effective span therefore which leads to an increase in lift and decrease in drag (Gursul et al., 2007). If we look at the line variation for the mean velocity magnitude plot, it can be noticed that there is a significant shift for injection cases compared to the baseline case.

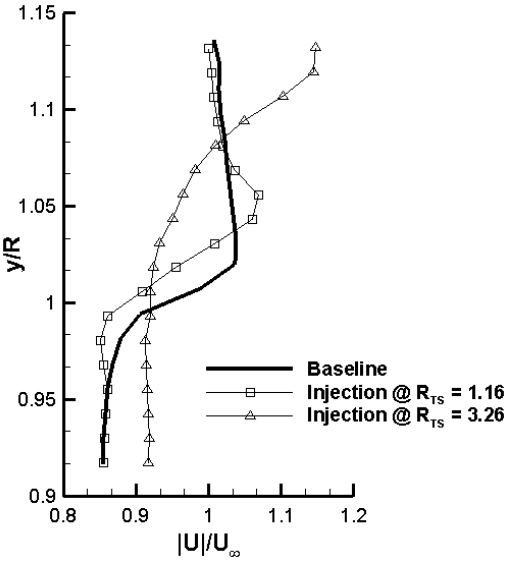

Figure 3. 11: Normalized mean velocity magnitude field comparison at x/R=0.31

3.2.2.2. Vorticity Field

The mean vorticity plots explain more clearly what happens to the tip vortex with injection around the tip flow. The tip vortex trajectory for the baseline case follows the wake boundary as it is found in the instantaneous vorticity plots. The center of the tip vortex core is aligned with the blade tip. Also, the strength of the tip vortex remains almost constant in the interrogation region and the tip vortex dominates the near wake. When it is looked at the injection case of R_{TS}=1. 16, the vortex center is shifted away from the blade tip and the wake boundary is thickened. As similar to the baseline case, in the injection at R_{TS}=1. 16, the tip vortex is still the dominant structure in the flow field but unlike the baseline case the tip vortex is disturbed. Moreover, the vortex structure found the tip vortex becomes more dissipative compared to the baseline case since the vorticity is getting reduced in the measurement domain. Also, an additional counter-rotating with smaller size and a weaker vortex trajectory is found at the upper side of the main vortex trajectory due

to jet flow mixing with the main flow. For the injection case of R_{TS}=3.26, it is found that the counter rotating vortex pairs have unequal strengths. According to Margaris (2010), the angle of attack between the jet and the local velocity affects the stability of the jet vortices and as the angle of attack increases the stability decreases (Margaris & Gursul, 2010). When we look at the Figure 3.9 to the maximum injection plot, the vortex pair at the lower section has lower vorticity compared to the upper pair. The measurements are performed at TSR=5 which is very close to design TSR value where angle of attack is very close to maximum lift coefficient, therefore the angle of attack is higher than 10-12 degrees (Ostovan, Hazaveh, & Uzol, 2013).

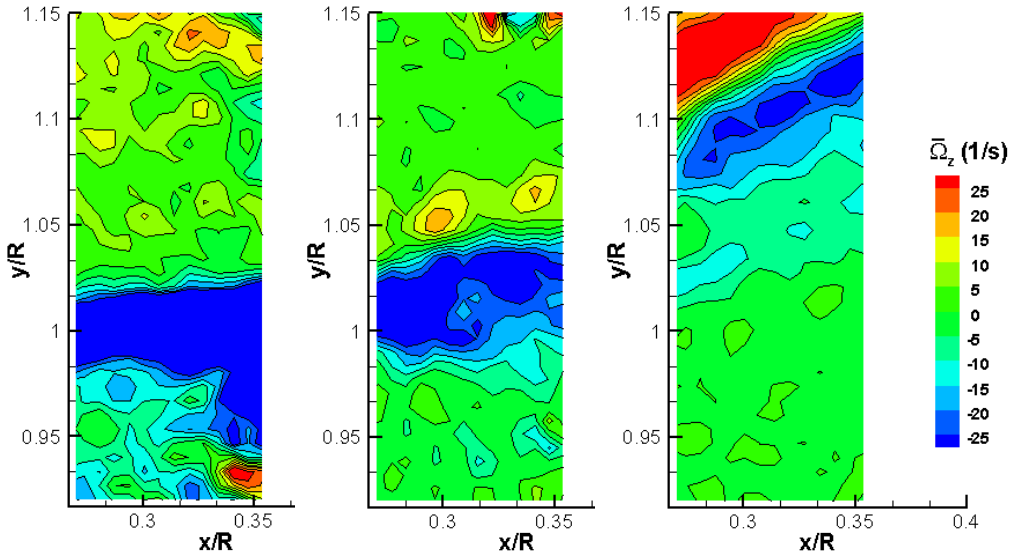

Figure 3. 12: Mean vorticity field comparison, *from left to right*: Baseline, R_{TS}=1.16 and R_{TS}=3.26

A similar comparison to the velocity fields is also performed for vorticity variations given in Figure 3.13 at axial location of x/R=0.28 and x/R=0.31. As it is expected, the highest peak occurs at baseline case due to the presence of a strong tip vortex. The negative vorticity at the y/R=1, indicates the direction of rotation which is in negative z/R direction or into the plane. Before and after the high peak region, the vorticity remains zero along the spanwise direction. For the injection case of R_{TS}=1.16, a negative double peak region is found for x/R=0.31. This double peak is due the irregularity of the tip vortex which is mixing with the injected flow. Also, it is seen that there is a positive vorticity region at y/R=1.07, where the second vortex with opposite rotational direction is introduced into the flow as it's explained previously. For x/R=0.28 location, there is only one vorticity peak region occur as similar to the baseline case with less vorticity and with larger area and higher location. In R_{TS}=3.26 case, double peak region with opposite vorticity signs are visible at x/R=0.28 location and also with unequal vorticity strengths as consistent with the contour plots. For x/R=0.31 location there is also a double peak region is found but at a higher radial location but this time the vorticity levels are also reduced compared to the closer axial location. According to the behavior of the vortex pair observed from contour plots, the vortex pair with positive direction of rotation will have a higher vorticity for R_{TS}=3.26 case and lower vorticity levels for R_{TS}=1.16 case compared to the other pair forming under it. The main reason for that is the mostly due to the difference between the strength of the jet velocities. For the minimum injection case, the injected air has a much smaller velocity compared to the maximum injection case and it mixes with the tip vortex as well as the freestream flow immediately by disturbing the structure of the tip vortex while the maximum injection case creates a strong obstacle between pressure and suction sides of the blade at the tip and almost prevents the formation of the tip vortex and remain strong for a longer while.

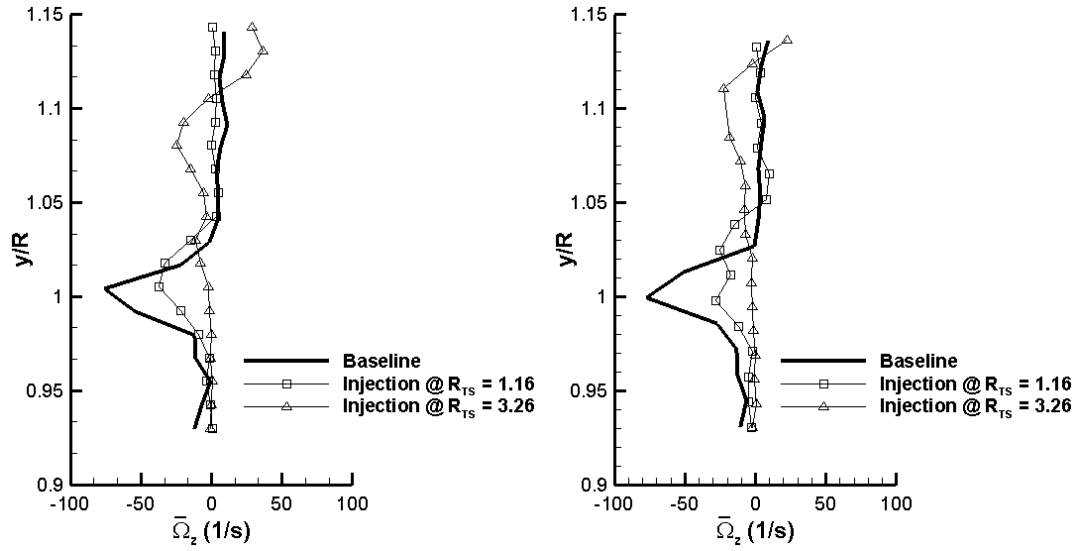

Figure 3. 13: Mean vorticity field comparison *left hand side* at x/R=0.28 and *right hand side* at x/R=0.31

Although it becomes very weak, it is quite obvious that the tip vortex keeps continue to shed despite high injection rate at R_{TS}=3.26. The explanation of this can be the location and size of the injection channel. The injection channel is a rectangular channel located on the chordline and closer to the leading edge of the blades and it occupies only the 29% of the chord. Therefore, there is a free space of 49% of the chord exists after the injection channel. So, a leakage still can occur during the operation of the wind turbine. This vortex shed from the trailing edge still interacts with the jet flow and follows the jet trajectory instead of following a regular trajectory similar to the baseline case. The schematic representation of the possible phenomenon is given in Figure 3.14. The jet flow exiting from the blade tips starts to dominate both main flow and the wake region of the wind turbine near the tip with an introduction of a counter-rotating vortex pair mentioned in instantaneous vorticity field. Results are in a good agreement with literature. Margaris and Gursul (2004)

showed that for low blowing rates, tip vortex and the jet vortex combine within a chordlength while for high blowing rates the stronger jet vortex appears away from the tip vortex which diffuses faster and follows the jet vortex trajectory (Margaris & Gursul, 2004).

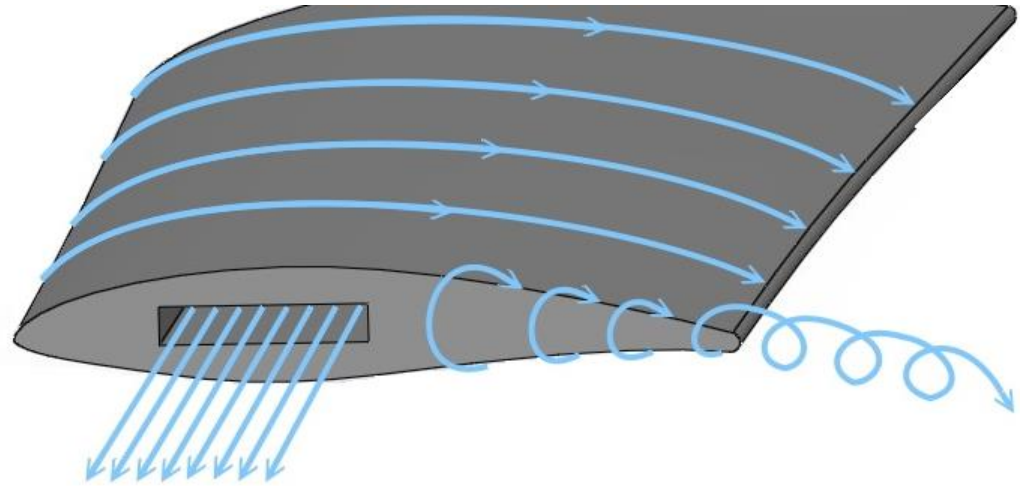

Figure 3. 14: Schematic representation of tip flow at injection ratio of R_{TS} =3.26

3.2.2.3. Turbulent Kinetic Energy Field

Turbulent kinetic energy variations given in Figure 3.15 are in good agreement with both velocity and vorticity contour plots discussed earlier. As it is expected the turbulent kinetic energy is higher where the tip vortex dominates the flow for baseline and R_{TS}=1.16 cases and where the injection dominates the flow for

R_{TS}=3.26 injection case. In other words the turbulent kinetic energy levels are higher where the turbulence effects are higher in the flow domain. The anomalies seen in the contour plots are due to the averaging and analysis errors and they have no physical meaning in the flow.

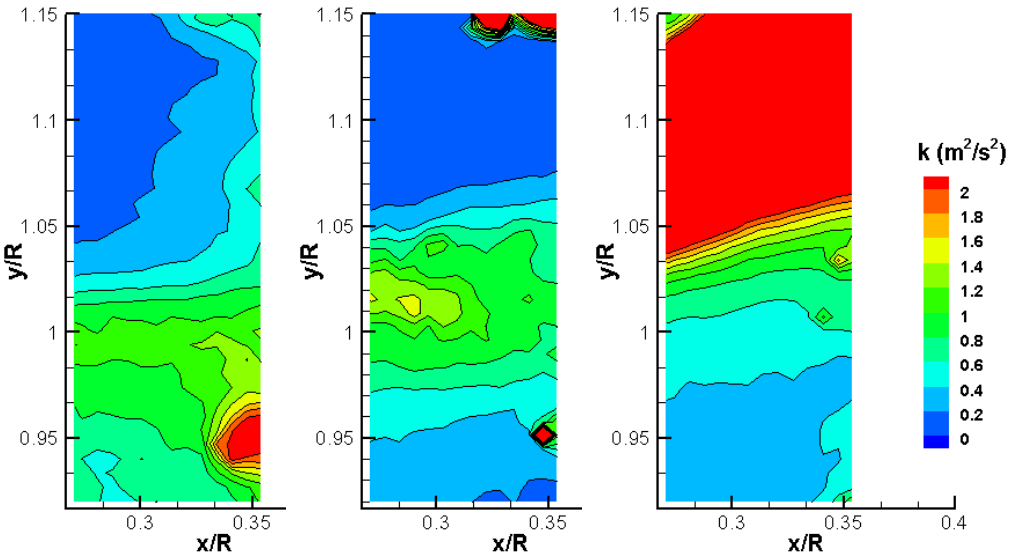

Figure 3. 15: Turbulent kinetic energy field comparison, *from left to right*: Baseline, R_{TS}=1.16 and R_{TS}=3.26

From the Figure 3.16, the line variations extracted along the x/R=0.31 are also good agreement with the velocity and vorticity field. Increase in the turbulent kinetic energy occurs where the tip vortex is dominant for baseline and minimum injection case and there is also very large increase found in maximum injection case where the highly turbulent jet flow region is created.

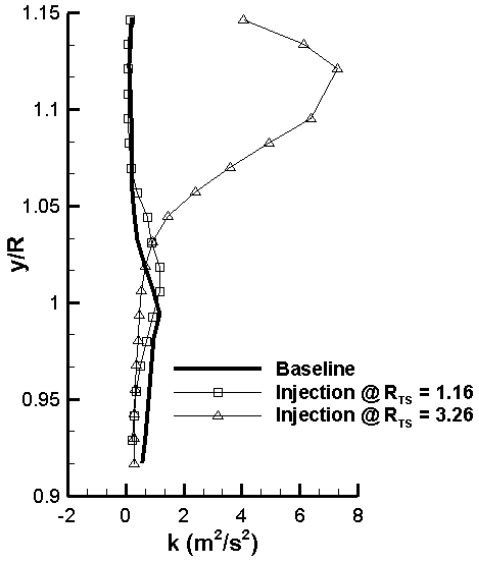

Figure 3. 16: Turbulent kinetic energy field comparison at x/R=0.31

3.2.2.4. Flow Angle Field

It is quite clear that with injection the expansion of the wake characteristics thus the flow angles are also changing. Flow angle field analysis is performed and given in Figure 3.17, to see how injection affects the flow angles therefore streamlines and dependently the wake expansion characteristics. As it can be seen from the contour plots there is a general trend found in previous comparisons. First of all, for baseline case the flow angles are higher at the wake region due to expansion of the wake as expected. This high angle region is reduced once we go away from the tip region where the flow recovers to the freestream flow conditions. In addition, flow angles are also started to get reduced when we go to the downstream of the rotor. A similar trend is also found for the R_{TS}=1.16 case with higher angles and also there is a shift in the high angle region. This region is concentrated around the tip region due to radial injection is introduced into the flow. Also, in this case we see a more disturbed

flow behavior compared to the baseline case which might be caused from the disturbed tip vortex structure. Again, in farther radial and also downstream axial locations, the flow angles are reduced. When we look at the maximum injection case we meet an entirely different field compared to the two other cases. The high speed injected flow dominates and changes the streamlines behind the rotor. The high angle field is very consistent with the results discussed earlier since the dramatic change in wake boundary, wake thickness and the velocity field behind the rotor should cause a change in the flow angles therefore streamlines as well. The highly turbulent jet exiting from the blade tips is extremely affects the flow field to follow its trajectory.

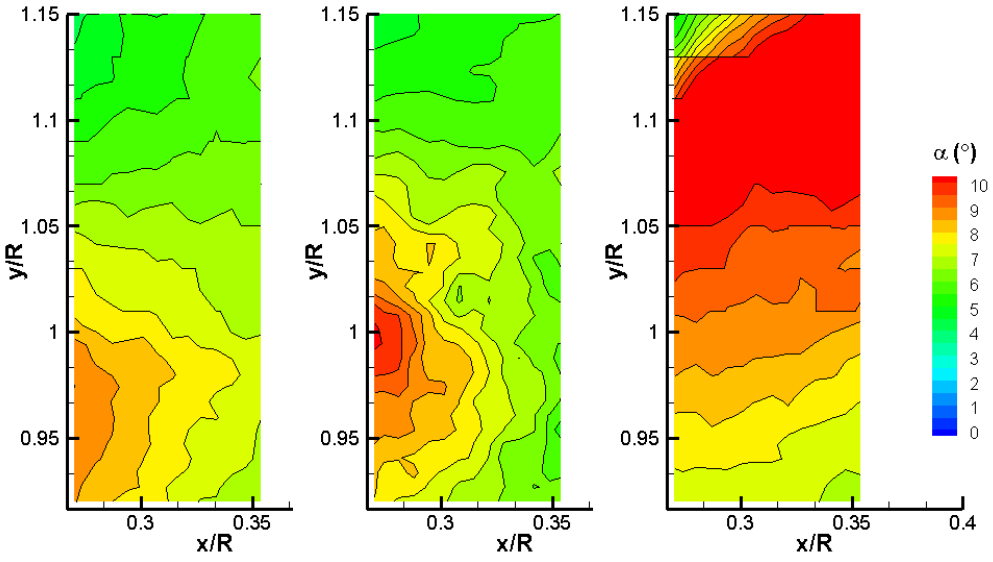

Figure 3. 17: Flow angle field comparison, *from left to right*: Baseline, R_{TS}=1.16 and R_{TS}=3.26

The change in flow angles in a fixed axial location at x/R=0.31 given in Figure 3.18, we see two distinct flow behavior. For baseline and minimum injection case, flow

angles behind the rotor are higher at the wake region and once we go away from the rotor tips it starts to reduce significantly. However, it is quite the opposite for the maximum injection case where the flow angles increase even more after the rotor and reaches a peak value around the center of the jet flow and after that point it starts to decrease. It can be seen that the R_{TS}=1.16 has two peak regions due to the irregular behavior of the disturbed vortex structure.

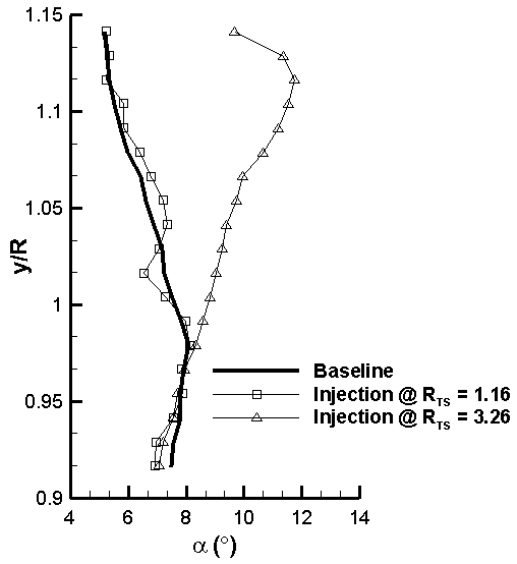

Figure 3. 18: Flow angle field comparison at x/R=0.31

3.3. Hotwire and PIV measurement comparison

A hotwire and PIV measurements for velocity field at baseline and injection scenario of R_{TS}=3.26 are performed in order to make a comparison between two different

measurement results. The hotwire measurements used for the comparison are taken with a single sensor Constant Temperature Anemometry (CTA) system. The data acquisition is done by connecting the sensor to a NI-9205 analog input module with NI DAQ-9172 chassis which are controlled by LabVIEW software program. Data are collected at a 2000 x 2000 mm^2 measurement area with sampling rate of 5 kHz and sampling time of 4 seconds with 2 x 10 mm^2 resolutions given in Figure 3.19. For more information it can be referred to Abdulrahim (2014). To be able to make a comparison directly, the hotwire data taken is trimmed according to the PIV measurement plane.

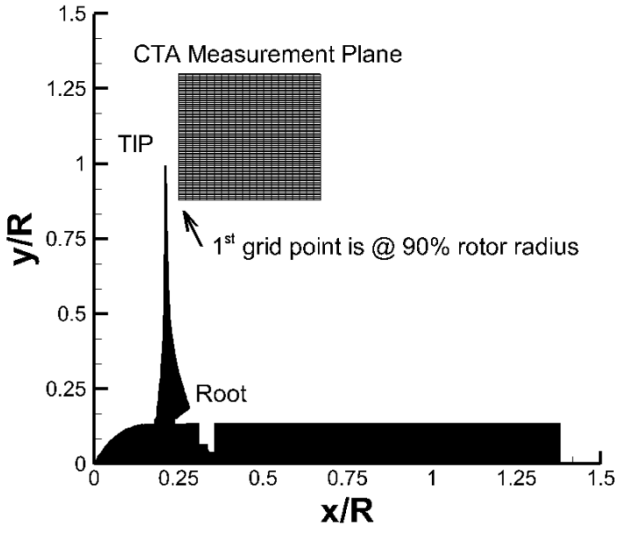

Figure 3. 19: CTA measurement plane (Abdulrahim, 2014)

Figure 3.20 presents the baseline, Figure 3.21 presents the injection scenario at R_{TS}=3.26 and Figure 3.22 gives the line variations, normalized according to the freestream velocity, along x/R=0.31 axial location comparisons between hotwire and PIV. Measurements are taken at same flow conditions as wind speed of 5 m/s and TSR=5. Hotwire and PIV measurements show a good agreement in terms of flow behavior, wake boundary region and behavior for both baseline and maximum injection scenarios. However, there is a difference in terms of velocity magnitude and the number of contours obtained from the measurements. These differences are mainly due to the differences in measurement resolutions. As it is mentioned in chapter two, PIV measurement resolution is 3.05 mm x 3.105 mm while hotwire resolution is 2 mm x 10 mm in x/R and y/R directions respectively. Another reason is that since the used hotwire probe is a single sensor probe which measures 1D component of the flow while PIV measures 2D characteristics.

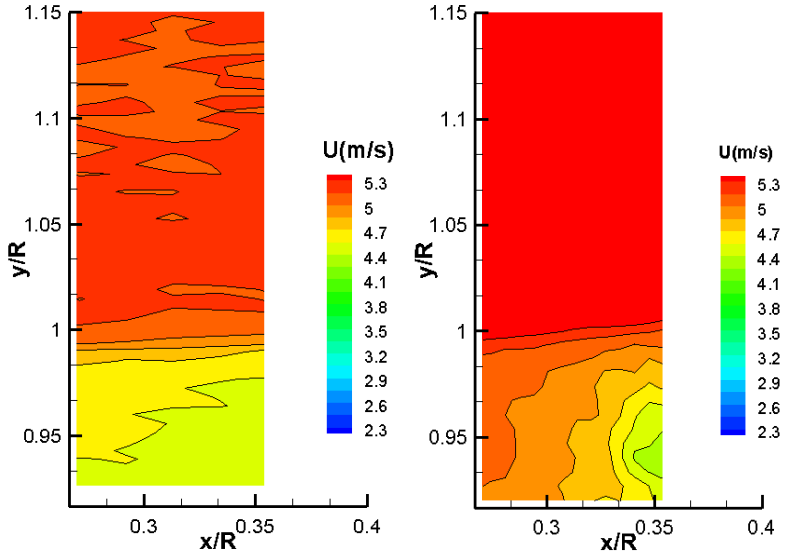

Figure 3. 20: Hotwire and PIV measurement comparison for baseline case at U_∞=5 m/s and TSR=5, *left hand side*: Hotwire *right hand side*: PIV measurement results

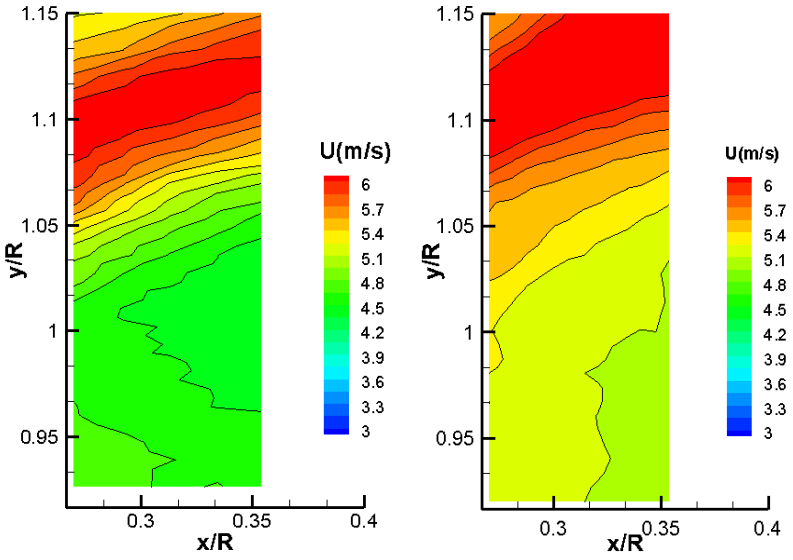

Figure 3. 21: Hotwire and PIV measurement comparison for R_{TS}=3.26 case at U_{∞}=5 m/s and TSR=5, *left hand side*: Hotwire *right hand side*: PIV measurement results

From the line variations given in Figure 3.22, the discrepancy introduced in contour plots are clearer especially for the main flow region farther from tip region. The main reason is mostly due to the resolution differences as mentioned. Also since the hotwire is sensitive to the ambient temperature, the measurements might be affected from the calibration of hotwire and temperature changes during the measurements. Beside these differences the results are quite similar for both PIV and hotwire measurements in given flow conditions.

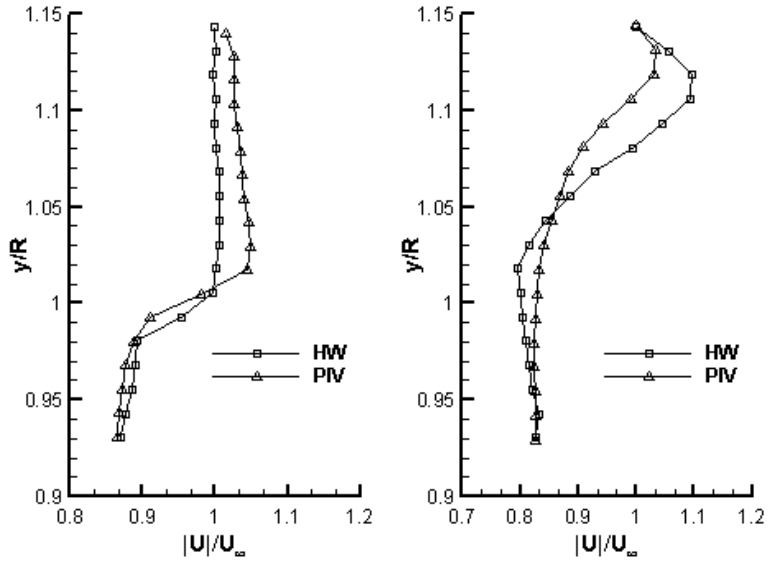

Figure 3. 22: Hotwire and PIV measurement line comparison at x/R=0.31at U_∞=5 m/s and TSR=5 for, *left hand side*: Baseline *right hand side*: R_{TS}=3.26 case

3.4. Power Budget Analysis

In the previous section, the effects of different injection cases are examined at a selected wind speed, TSR ratio and for baseline and two injection scenarios. In this section a power budget analysis will be performed in order to understand the feasibility and efficiency of the injection on the performance characteristics for this specific model wind turbine.

The effects of injection on performance characteristics of the model wind turbine used in this study are presented for two different wind speeds and for baseline and three different injection scenarios (Abdulrahim, 2014)(Anik et al., 2014). To be able to see the relation between performance coefficients and the injection ratios, C_P and C_T versus R_{TS} graphs are plotted at TSR=5 for 5 m/s wind speed shown in Figure

3.23 where the injection has the largest impact on load coefficients of the model wind turbine. If we look at both graphs, in general both C_P and C_T are increasing with increasing injection ratio as expected and found in power and thrust curves. However this increase has different trends for both power and thrust coefficients. For power curve, C_P values first increase linearly with increasing injection ratio up to R_{TS}=2.45 then, at R_{TS}=3.26 a sudden jump occurs. The increase of the C_P value is around 8% from baseline to R_{TS}=1.16 and from R_{TS}=1.16 to R_{TS}=2.45 while increase from R_{TS}=2.45 to R_{TS}=3.26 is almost 29%. Secondly, for the thrust curve, the behavior is more irregular. From baseline to R_{TS}=1.16, it starts with a higher increase compared to C_P from baseline to injection case of R_{TS}=1.16 and then from R_{TS}=1.16 to R_{TS}=2.45, it shows a very little increase and finally from R_{TS}=2.45 to R_{TS}=3.26 there is a jump in the C_T value similar to the power coefficient. In both graphs, one can say that if we look at overall trend, there is a non-linear relation between performance characteristics and injection ratio. In addition, injection effects power coefficient more than it's affecting the thrust coefficient.

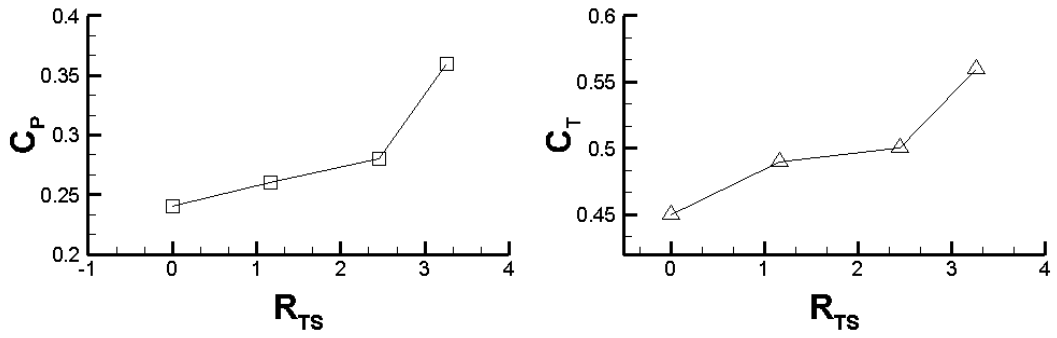

Figure 3. 23: Variation of C_P and C_T with R_{TS} for baseline and three different injection scenarios at 5 m/s for TSR=5.

The ultimate goal of applying an AFC method is to extract the maximum outcome with adapting in a change in conditions. Therefore, the main reason to perform this analysis is to find an optimum condition to apply injection ratio in sense of getting the optimum benefit from it. Since the TSR is one of the most important parameter of the wind turbines, this analysis is also helpful in terms of scaling between the model and a real turbine.

The power budget analysis presented in this section is defined as the difference between wind power obtained with injection and the power spend to injection and the baseline power measured over the baseline power measured, defined in equations from [3.1] to [3.3]. This analysis reveals the effectiveness of the tip injection changes according to the changing injection ratios and TSR values. Therefore, it shows an insight about how to apply and how to control the tip injection to extract maximum benefit with minimum energy.

$$PB = \frac{(P_{INJ} - P_{BL}) - P_{jet}}{P_{BL}} \quad [3.1]$$

$$P_{INJ} = \frac{1}{2}\rho A U_{\infty}^{3} C_{PINJ} \quad [3.2]$$

$$P_{Jet} = \frac{1}{2}\rho A U_{Jet}^{3} \quad [3.3]$$

Figure 3.24 and 3.25 gives the results of analysis of the power budget analysis explained above for wind speed of 5 m/s and 6 m/s respectively. The analysis presents an interesting result for both wind speeds. As it is examined, the power increase obtained with injection mostly appears as a power deficiency since according to the calculations we have to spend more energy to injection than we are

gaining with the injection. If we look in more detail, one can notice that this deficiency increases with increasing injection ratio for 5 m/s and 6 m/s wind speed cases.

For the 5 m/s wind speed case, only injection ratio of R_M=0.3% give positive values after TSR value of 3.5. The power efficiency for this case has a maximum value around TSR= 4.5 which is very close to the design TSR value. For the other two injection cases, all analysis gives a power deficiency. It can be noticed that for low TSR values for less than 3.5, injection has a deficiency values more that 100% especially for the maximum injection case since at low tip speed ratios injection has no effect on power characteristics (Abdulrahim, 2014)(Anik et al., 2014).

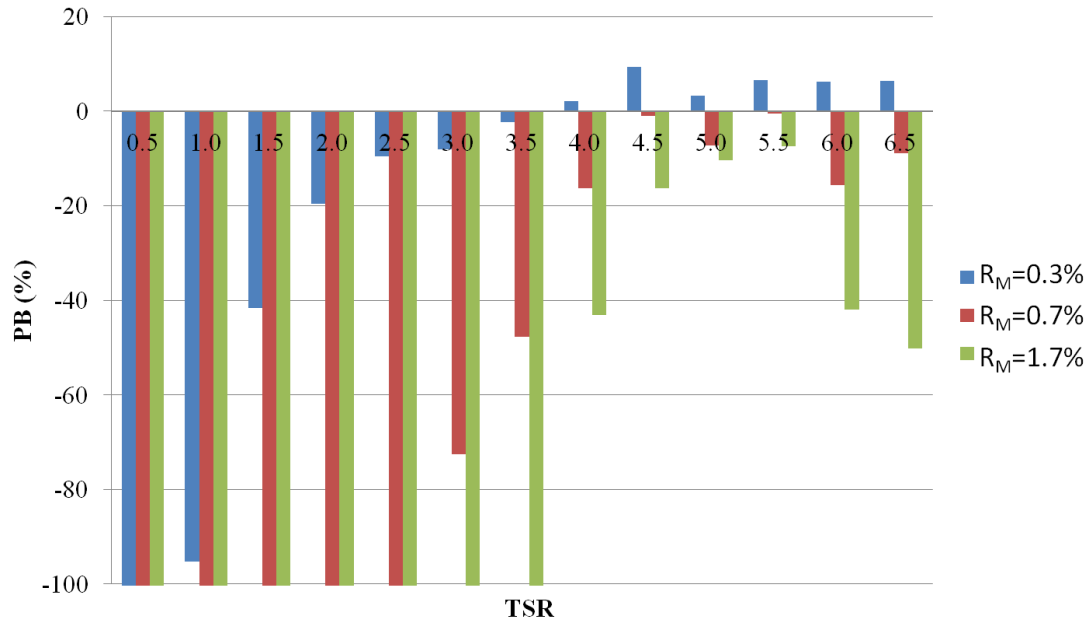

Figure 3. 24: Power budget analysis for three different injection ratios at 5 m/s wind speed

For the 6 m/s wind speed case, all injection cases appear as a power deficiency and this deficiency increases with increasing injection ratio similar to the 5 m/s case. Power deficiency exceeds 100% for low TSR values again mostly for maximum injection case and then the deficiency starts to decrease around the design tip speed ratio for all cases where all the injection has the major impact on power coefficient.

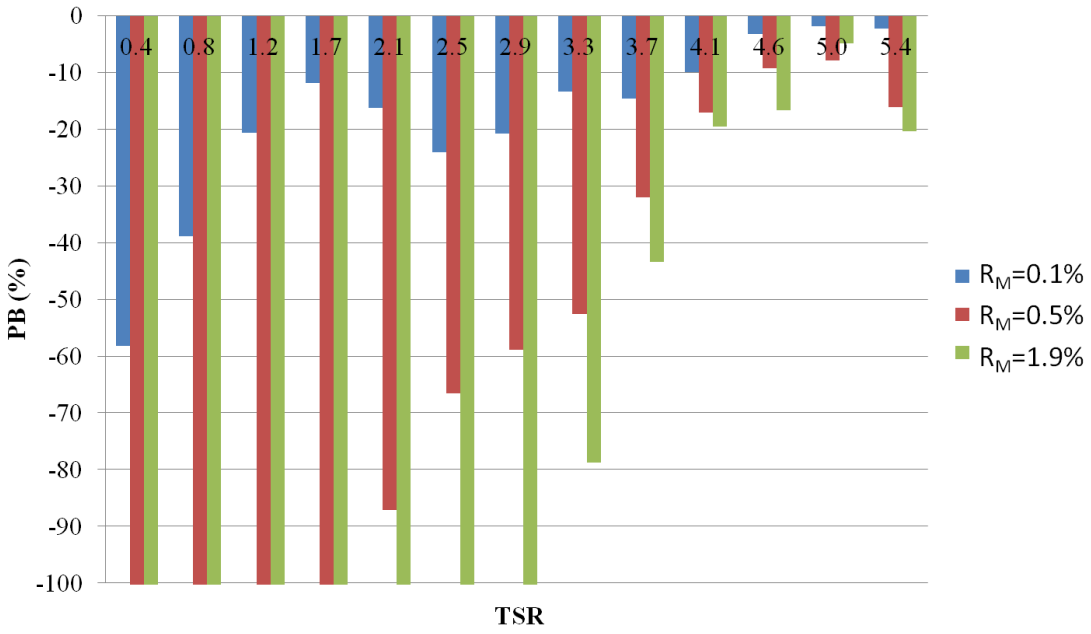

Figure 3. 25: Power budget analysis for three different injection ratios at 6 m/s wind speed

It will not wrong to mention that, the power deficiency at low TSR values is a result of the operating conditions of the wind turbine. Since angles of attack are quite high

at this region, the blades are not able to produce enough lift therefore they produce very small amount of power. In other words, due to high angles of attack the boundary layer is already separated from the surface so the blades are in stall condition. So, in this region where TSR values are below design TSR, tip leakage may not be a major issue. At this point, using injection most probably will not provide any benefit especially in power characteristics. On the other hand, the small amount of increase in the thrust value shows that injection can be still effective at stall condition since it also causes an increase the loads. It is shown that, at high TSR values, for 5 m/s wind speed, only the smallest injection ratio seems to be promising in terms of power gain. The other injection scenarios for 5 m/s affect negatively the system in terms of flow efficiency. For 6 m/s none of the injection ratios are able to provide a power gain to the system. However, it can be said that injection is able to increase the loads on the wind turbine rotor and it is also affecting the flow field around the wind turbine and. Increasing loads on the rotor may be beneficial in terms of wind turbine wake interactions between successively arranged wind turbines due to changes occur in the wake section due to injection.

3.5. Mass Flow Analysis

In this section a combined preliminary mass flow analysis is performed for the results obtained from both power budget analysis and tip flow field measurements in order to give a better insight to the phenomenon. The main purpose of this study is to find a relationship between the performance and the tip flow characteristics.

Although, the injection causes a deficiency for the system, it increases the power and thrust generated by this model turbine after a certain TSR value. According to the study of Gursul et al. (2007), blowing in the span direction increases the effective span therefore aspect ratio of the wing as mentioned earlier (Gursul et al., 2007). It is well known that the power generated by a wind turbine is a function of area of the rotor and the velocity of the wind. From conservation of mass, total mass flow rate through the rotor disk should be conserved in the axial direction. From equation [3.4]

and the control volume represented in Figure 3.26, the mass flow rate behind the rotor should be equal to the mass flow rate passing through the rotor and be preserved through the wake. If we consider only the axial flow along the stream tube and assume that the spanwise injection is only effective in lateral direction therefore it has no contribution to the axial flow, we can say that the power and thrust generation of the model wind turbine is strongly dependent on axial mass flow rate. When it is examined the PIV results, there is a significant enlargement in wake radius behind the rotor. This growth in wake radius increases with increasing injection rate. Since the momentum is proportional with square of the radius of the wake, an increase in radius will cause an increase in the momentum in the order of its square.

$$\dot{m} = \rho u A = \rho u_1 A_1 \qquad [3.4]$$

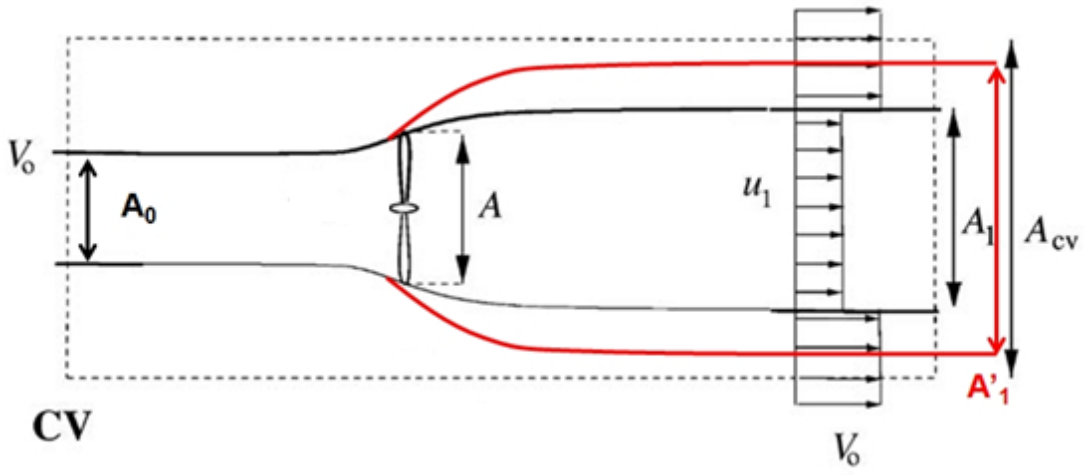

Figure 3. 26: Control volume analysis (Hansen, 2008).

From the PIV results of mean velocity field, the amount of expansion in the wake region is performed in terms of increase in effective span and the average velocity behind the wake. For injection case of R_{TS}=1.16 and R_{TS}=3.26, the increase in effective span is calculated as roughly 3.36% and 10.03% compared to the baseline respectively. A representation for the amount of area increase is given in Figure 3.27 for all cases where the black solid line represents the geometrical rotor area. If we consider the density and the velocity behind the wake are constant, the amount of increase in mass flow rate is calculated as 6.84% and 21.07% for injection case of R_{TS}=1.16 and R_{TS}=3.26 respectively. From the conservation of mass flow rate, very basically we can relate the amount of power generated by the rotor to the mass flow rate passing through it given in equation [3.5]. From load measurements it is known that at 5 m/s wind speed and for TSR=5, the amount of increase in the power generated is 5.94% and 48.15% for minimum and maximum injection scenarios. With a simple calculation the amount of increase in radius, increases the power in order of increase in mass flow rate. However, this increase in mass flow rate based on only radius increase does not seem to enough to create that amount of power increase for the maximum injection case. On the other hand, the amount of increase in effective span is seem to enough to explain in increase in power for the R_{TS}=1.16 case.

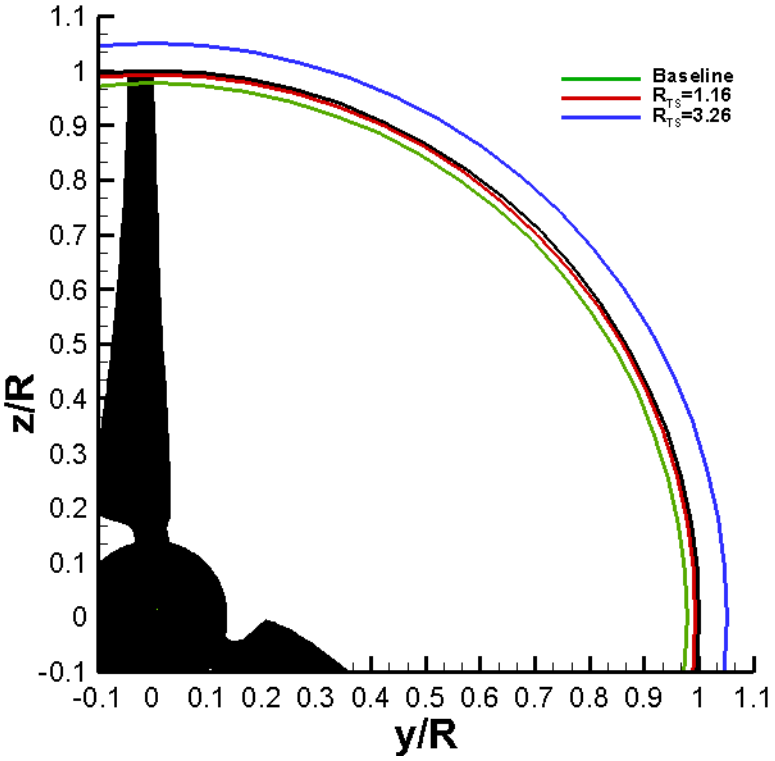

Figure 3. 27: Effective span comparison

$$P = \frac{1}{2}\rho A_1 u_1^3 = \frac{1}{2}\dot{m}u_1^2 \qquad [3.5]$$

The increase happening in the flow angles presented therefore in the wake expansion can be related to the increase in thrust coefficient as well with injection on this model wind turbine (Anik et al., 2014). If we simply consider the control volume analysis given in Figure 3.26, the upstream area cannot be affected from the tip injection therefore it should be remain constant. However, there is a sudden expansion in the streamtube represented with red lines in Figure3.26, which results in a larger wake area far downstream of the turbine. Therefore there should be an increase in

incoming flow velocity which causes an increase in velocity. From the thrust formula for the 1D momentum analysis given in equation [3.6], if we consider for far upstream velocity V_0 and velocity behind the wake are not changing, the only changing parameter is the effective area of the rotor due to the increase in effective span. Therefore the mass flow rate is also increases as it is explained and found as 6.84% for R_{TS}=1.16 and 21.07% for R_{TS}=3.26. The amount of increase in thrust is calculated as 8.89% and 24.40% for minimum and maximum injection cases for given conditions. According to the calculations, the amount of increase in effective span can explain the thrust increase in terms of increase in mass flow rate coming through the rotor.

$$T = \rho u A (V_0 - u_1) \qquad [3.6]$$

In addition, for injection case of R_{TS}=3.26 the velocity behind the rotor also increases according to the PIV measurements. The velocity affects the power more than radius increase because power production is proportional with the cube of the velocity. The velocity increase behind the rotor around the tip region is calculated as 9.64% for maximum injection case for the given area of measurement. It can be remembered that there was no significant increase for the minimum injection case. Therefore, when the velocity increase is taken into account, the amount of increase in the power becomes 32.67% for the injection case of R_{TS}=3.26. These calculations show that a very large amount of power increase due to injection can be related to the axial mass flow rate. The amount of increase in thrust also depends on the velocity increase. Accordingly, increase in thrust with the increase in velocity will contribute to thrust in amount of equal to 24.78% in total which is also consistent with the total increase in thrust coefficient for maximum injection case. Therefore, power and thrust characteristics as well as the axial mass flow rate characteristics changes in the near flow field which indicates that a change must be occur to the stream tube around the wind turbine with injection. So, it can be concluded from the results that injection

does not only increase the effective span but also effects the flow behind the rotor and cause an acceleration in the wake velocity which results in an increase in overall power and thrust generation of the model turbine. This result leads that although it appears as a power deficiency for most of the cases that have been investigated, injection can be still useful in terms of decreasing the negative effects of the rotor wake on downstream rotors in a wind farm which can lead an overall increase of the wind farm efficiency in total.

CHAPTER 4

CONCLUSION

In this study effect of spanwise steady injection from the tips of a model wind turbine is examined in terms of tip flow field characteristics at selected flow and injection conditions as well as the power budget and 1D mass flow analysis in terms of turbine performance. Measurements performed in front of an open-jet wind tunnel exit. The model wind turbine is a horizontal axis wind turbine with three bladed rotor which is a replica of the turbine rotor geometry used in blind tests in NTNU. The blades have NREL S826 airfoil profile. The model turbine is designed to achieve tip injection from the blades while it's rotating.

Tip flow field measurements are performed using a Time Resolved Particle Image Velocimetry system at a horizontal plane located at tip section. Power budget calculations for the performance of the model turbine for feasibility analysis as well as simple 1D mass flow conservation analysis is performed according to PIV measurements in order to understand the relationship between the performance and the tip flow characteristics of the model turbine.

Injection system used consists of a specially designed and sealed with special mechanical seals that allow rotation and prevent air leakage, pressure chamber, a hollow shaft, a pressurized hub and special blades with air channels embedded inside. In order to understand the effects of tip injection two different injection ratios has been selected for flow field, which are the minimum and maximum ratios used for performance measurements in previous studies.

PIV measurements are performed to understand the flow physics lies behind the performance increase. Raw images of the instantaneous flow field that obtained from measurements are used for flow visualization to give qualitative understanding about the tip vortex characteristics. Analysis results of the flow filed also presented for both instantaneous and mean flow characteristics. Velocity, vorticity, turbulent kinetic energy and flow angle fields are examined to see the effects of tip injection on the tip vortex characteristics. It is found that depending on injection ratio tip flow field characteristics therefore tip vortex characteristics such as core size, vorticity, location and dissipation characteristics as well as wake characteristics such as wake thickness, expansion characteristics and wake velocity levels can be changed. In addition, results obtained for this study has also been compared with hotwire measurements performed for another study and the findings are discussed.

Power budget calculations shows that although the power and thrust generation is increases with increasing injection ratio, using injection creates a power deficiency in terms of flow power except for 5 m/s at minimum injection ratio. It is also found that any injection ratio used at 6 m/s does not seem to be effective as in the 5 m/s also, they are feasible in terms of power budget.

As final concluding remarks; there is no doubt that tip injection affects the tip flow characteristics therefore the wake of the turbine as shown in PIV results. It does not just change the tip vortex characteristics, but it also changes the wake characteristics in terms of wake boundary, expansion and wake velocity. It needs to be accounted that despite the power deficiency of the tip injection on this model turbine, it still can be beneficial in terms of downstream turbines which are successively arranged in a wind farm. The main reason to use an active flow control method is to use it when it is needed. Usually, it is well known that downstream turbines are suffering from the velocity reduction due to wake of the upstream rotor. In a wind farm, the energy loss which is called as array losses is a function of wind turbine spacing and operating characteristics, there must be a specific distance between the wind turbines where the flow velocity behind the wake recovered to a reasonable value to reduce the severe effects of its wake (Manwell, J. F. et al., 2009). This limits the capacity of the wind

farms in terms of both number of turbines and the total amount of energy produced. Therefore, even though it creates a power deficiency, injection might still increase the total amount of energy generated in a wind farm and can change the entire structure of it. In order to understand the effects of tip injection better, this study needs to be expanded in a way that:

- PIV measurements should be done at different wind speeds for different TSR values at different injection scenarios in order to fully understand how, when and why injection affects the performance characteristics in a way that is presented.
- A complete flow field analysis should be done around the rotor blade and the near wake to resolve the entire flow filed and how it changes with injection in terms of seeing the effects on the flow around the rotor and moreover to discover the physical phenomenon.
- Phase-locked PIV measurements at the tip section should be done to resolve better the tip vortex characteristics with and without injection.
- Performance measurements with power budget calculations should be expanded in terms of flow velocity, TSR as well as number of different injection scenarios therefore new and strong blades should be manufactured.
- Effects of tip injection on the performance characteristics of a downstream rotor should be studied to see its feasibility in terms of rotor wake interactions for successively placed wind turbines.

REFERENCES

Abdulrahim, A. (2014). *Experimental Investigation of the Effects of Tip-Injection on the Aerodynamic Loads and Wake Characteristics of a Model Horizontal Axis Wind Turbine Rotor*.

Adaramola, M. S., & Krogstad, P.-Å. (2011). Experimental investigation of wake effects on wind turbine performance. *Renewable Energy*, *36*(8), 2078–2086. doi:10.1016/j.renene.2011.01.024

Anik, E., Abdulrahim, A., Ostovan, Y., Mercan, B., & Uzol, O. (2014). Active control of the tip vortex: an experimental investigation on the performance characteristics of a model turbine. *Journal of Physics: Conference Series*, *524*(2004), 012098. doi:10.1088/1742-6596/524/1/012098

Bai, Y., Ma, X., & Ming, X. (2011). Lift enhancement of airfoil and tip flow control for wind turbine. *Applied Mathematics and Mechanics*, *32*(7), 825–836. doi:10.1007/s10483-011-1462-8

Duraisamy, K., & Baeder, J. D. (2006). Numerical Simulation of the Effects of Spanwise Blowing on Wing-tip Vortex Formation and Evolution. *Journal of Aircraft*, *43*(4), 996–1006. doi:10.2514/1.19746

Gaunaa, M., & Johansen, J. (2007). Determination of the Maximum Aerodynamic Efficiency of Wind Turbine Rotors with Winglets. *Journal of Physics: Conference Series*, *75*, 012006. doi:10.1088/1742-6596/75/1/012006

Geng, S., Zhang, H., Chen, J., & Huang, W. (2007). Numerical Study on the Response of Tip Leakage Flow Unsteadiness to Micro Tip Injection in a Low-Speed Isolated Compressor Rotor. In *ASME Turbo Expo 2007: Power for Land, Sea and Air*. Montreal, Canada.

Greenblatt, D. (2012). Fluidic Control of a Wing Tip Vortex. *AIAA Journal*, *50*(2), 375–386. doi:10.2514/1.J051123

Gursul, I., Vardaki, E., Margaris, P., & Wang, Z. (2007). Control of Wing Vortices, 137–151.

Han, Y. O., & Leishman, J. G. (2004). Investigation of Helicopter Rotor-Blade-Tip-Vortex. *AIAA Journal*, *42*(3), 524–535.

Hansen, M. O. L. (2008). *Aerodynamics of Wind Turbines* (Second Edi.).

Heyes, A. L., & Smith, D. A. R. (2004). Spatial perturbation of a wing-tip vortex using pulsed span-wise jets. *Experiments in Fluids*, *37*(1), 120–127. doi:10.1007/s00348-004-0791-5

Heyes, F. J. G., & Hodson, H. P. (1993). Measurement and Prediction of Tip Clearance Flow in Linear Turbine Cascades. *Journal of Turbomachinery*, *115*(July), 376–382. doi:03 Aug 2011

Johansen, J., & Sørensen, N. N. (2006). *Aerodynamic investigation of Winglets on Wind Turbine Blades using CFD*.

Liu, Z., Russell, J. W., & Sankar, L. N. (2001). A Study of Rotor Tip Vortex Structure Alteration Techniques Introduction. *Journal of Aircraft*, *38*(3).

Liu, Z., Sankar, L., & Hassan, A. (2000). Alteration of the tip vortex structure of a hovering rotor using oscillatory jet excitation. *38th Aerospace Sciences Meeting and Exhibit*, 1–9. doi:10.2514/6.2000-259

Lu, X., Chu, W., Zhu, J., & Tong, Z. (2006). Numerical and Experimental Investigations of Steady Micro-Tip Injection on a Subsonic Axial-Flow Compressor Rotor. *International Journal of Rotating Machinery*, *2006*, 1–11. doi:10.1155/IJRM/2006/71034

Manwell, J. F., McGowan, J. G., & Rogers, A., L. (2009). *Wind Energy Explianed: Theory, Design and Application*.

Margaris, P., & Gursul, I. (2004). Effect of Steady Blowing on Wing Tip Flowfield. In *2nd AIAA Flow Control Conference*. Portland, Oregon.

Margaris, P., & Gursul, I. (2010). Vortex topology of wing tip blowing. *Aerospace Science and Technology*, *14*(3), 143–160. doi:10.1016/j.ast.2009.11.008

Matalanis, C. G., Nelson, G. D., & Eaton, J. K. (2007). Novel Aerodynamic Device for Wake Vortex Alleviation. *AIAA Journal*, *45*(9), 2350–2352. doi:10.2514/1.30124

Mercan, B. (2012). *Experimental Investigation of the Effects of Waveform Tip Injection on the Characteristics of Tip Leakage Vortex in a LPT Cascade*.

Mercan, B., Doğan, E., Ostovan, Y., & Uzol, O. (2012). Experimantal Investigation of the Effects of Waveform Tip Injection in a Low Pressure Turbine Cascade. In *ASME Turbo Expo* (pp. 1–13). Copenhagen, Denmark.

Micallef, D., Akay, B., Sant, T., Ferreira, C. S., & Van Bussel, G. (2011). Experimental and numerical study of radial flow and its contribution to wake development of a HAWT. *European Wind Energy Conference and Exhibition 2011, EWEC 2011*, 166–170. Retrieved from http://www.scopus.com/inward/record.url?eid=2-s2.0-84870196535&partnerID=40&md5=b67f3b97cf6092ee9dc0cef017212e41

Nie, C., Tong, Z., Geng, S., Zhu, J., & Huang, W. (2006). Experimental Investigations of Micro Air Injection to Control Rotating Stall.pdf. *Journal of Thermal Science*, *16*(1), 1–6.

Ostovan, Y. (2011). *Experimental Investigation of Waveform Tip Injection on the Characteristics of the Tip Vortex*.

Ostovan, Y., Hazaveh, H. A., & Uzol, O. (2013). A Comprehensive Aerodynamic Characterization Study for the NREL S826 Airfoil at Low Reynolds Numbers.

Panagakos, A., & Lee, T. (2006). Tip Vortex Control via an Active Trailing-Edge Tab. *Journal of Aircraft*, *43*(4).

Ragheb, M., & Ragheb, A. M. (2011). Wind Turbines Theory - The Betz Equation and Optimal Rotor Tip Speed Ratio. In R. Carriveau (Ed.), *Fundamental and Advanced Topics in Wind Power*. Retrieved from www.intechopen.com/books/fundamental-and-advanced-topics-in-wind-power/wind-turbines-theory-the-betz-equation-and-optimal-rotor-tip-speed-ratio

Shen, W. Z., Mikkelsen, R., Sørensen, J. N., & Bak, C. (2005). Tip loss corrections for wind turbine computations. *Wind Energy*, *8*(4), 457–475. doi:10.1002/we.153

Shimizu, Y., Imamura, H., Matsumura, S., & Maeda, T. (1995). Power Augmentation of a Horizontal Axis Wind Turbine Using a IVlie Type Tip Vane : Velocity Distribution Around the Tip of a HAWT Blade With and Without a Mie Type Tip Vane, *117*, 297–303.

Shimizu, Y., Ismaili, E., Kamada, Y., & Maeda, T. (2003). Rotor Configuration Effects on the Performance of a HAWT With Tip-Mounted Mie-Type Vanes. *Journal of Solar Energy Engineering*, *125*(4), 441. doi:10.1115/1.1621671

Somers, D. M. (2005). The S825 and S826 Airfoils Period of Performance : 1994 – 1995.

Uzol, O., Brzozowski, D., Chow, Y.-C., Katz, J., & Meneveau, C. (2007). A database of PIV measurements within a turbomachinery stage and sample comparisons with unsteady RANS. *Journal of Turbulence*, *8*, N10. doi:10.1080/14685240601142867

Vasilescu, R. (2004). *Helicopter Blade Tip Vortex Modification In Hover Using Piezoelectrically Modulated Blowing*. Georgia Institute of Technology.